
Integrating Quantitative Mineral Texture Measurements into the ARD Characterisation Protocol for Improved Accuracy in ARD Characterisation and Prediction

*Report to the
Water Research Commission
Prepared by the Minerals to Metals Initiative,
University of Cape Town*

**O Guseva, AKB Opitz, JL Broadhurst,
STL Harrison & M Becker**

WRC Report No. 2846/1/22
ISBN 978-0-6392-0498-7

September 2022



Obtainable from

Water Research Commission

Private Bag X03

Gezina

PRETORIA, 0031

orders@wrc.org.za or download from www.wrc.org.za

DISCLAIMER

This report has been reviewed by the Water Research Commission (WRC) and approved for publication. Approval does not signify that the contents necessarily reflect the views and policies of the WRC, nor does mention of trade names or commercial products constitute endorsement or recommendation for use.

Research Highlights

Integrating quantitative mineral texture measurements for improved accuracy in characterisation and prediction of acid rock drainage from waste rock

Using a waste rock case study from an African orogenic gold deposit (one pyrite-bearing sample and one pyrrhotite-bearing sample)

ARD characterisation on the micro particle scale (<1 mm)



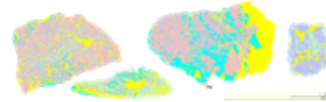
Predominantly liberated Fe-sulfides

- Static tests (ANC, MPA, NAG)
- UCT batch biokinetic test



Accompanied by detailed analyses of particle size distributions, elemental grades (XRF, LECO) mineral grades, mineral liberation and association (QEMSCAN, QXRD)

ARD characterisation on the meso particle scale (>1 mm)



Predominantly unliberated Fe-sulfides

- Humidity cell kinetic test run over 52 weeks



Quantification of mineral grades supported ARD classification (PAF, NAF, UC)

Quantification of the mineral liberation and association characteristics did not change the interpretation but added more certainty and accuracy to the waste rock classification

Quantification of bulk mineral grades and mineral grade on a particle size-by-size basis was central to the interpretation of the humidity cell test results

Quantification of mineral liberation and association characteristics of Fe-sulfide and carbonate minerals on a particle size-by-size basis was central to the interpretation of the humidity cell test results providing more certainty and accuracy to the waste rock classification

African case study presented alongside results of 3 independent international case studies showcasing the value of integrating mineral texture measurements with standard ARD assessment tools

A recommendation that the inclusion of mineral texture measurements on a particle size-by-size basis becomes mandatory for standard ASTM humidity cell testing

This page was intentionally left blank

Executive Summary

Today more than ever, minerals and metals play a critical role in our modern society. Mining is not a waste-free process and a significant amount of material is deposited onto waste rock dumps. These dumps are often associated with acid rock drainage (ARD) resulting in the acidification of local water alongside high sulfate concentrations and elevated levels of deleterious metals – making this water unfit for human consumption and destructive to the surrounding environment. ARD occurs through the combined effects of acid formation and neutralisation reactions, specifically through the oxidation of metal sulfide minerals, dissolution of gangue minerals (such as various carbonate and silicate minerals) and release of deleterious metals into freshwater systems. In addition to the mineralogy, the type of oxidant, pH, climate and the presence of naturally occurring bacteria all affect ARD generation.

The ARD potential of waste rock is assessed using geochemical static and kinetic characterisation and prediction tests. Although these tests may be accurate, in some cases they fail to adequately characterise and predict the ARD potential of mining waste due to the inherent complexity of the mechanisms associated with ARD formation and an incomplete understanding of the governing factors. It has been argued that the role of mineral and texture (the interrelationship of different mineral grains with one another) quantification has been undervalued in ARD testing protocol and its integration is essential to facilitate the understanding and enhancement of existing test methods. The potential techno-economic, environmental and social consequences of not improving existing test methods can be significant by either over- or under engineering for ARD prevention and mitigation.

Recent advancements in mineral texture quantification arising from allied fields of mineral processing and metallurgy create an opportunity to systematically investigate the integration of mineral and texture quantification into the ARD assessment toolbox. The overarching objective of this study is to quantitatively evaluate the role of mineralogy and texture in the context of commonly practiced ARD characterisation and prediction tests on micro (<1mm) and meso scale (>1mm) material. This objective can be further broken down into the following aims:

- (a) To quantify the effect of mineral texture on ARD characterisation on the micro scale (specifically in the context of small-scale laboratory static and biokinetic tests).
- (b) To quantify the effect of mineral texture on ARD characterisation on the meso scale (specifically in the context of small-scale laboratory kinetic tests).
- (c) To develop the case study supporting a recommendation to prescribe integration of mineral textural information into the larger context of global protocol on ARD characterisation and prediction.

Two waste rock samples from an African orogenic gold deposit have been studied extensively using a combination of standard static ARD characterisation tests (ABA, NAG, NAPP, as well as the UCT biokinetic test), and kinetic humidity cell characterisation and prediction tests accompanied by detailed quantitative mineralogical analysis of particle mineral-textural properties in a series of discrete size fractions using automated SEM-EDS (QEMSCAN).

Static ARD characterisation tests classified sample B as potentially acid forming and sample C as uncertain. Quantitative analysis of the mineral grades confirmed this classification due to the greater content of Fe sulfide (dominantly pyrite) than carbonate minerals in sample B. For sample C, the uncertain classification was supported by the mineralogy, which indicated both a high content of carbonate and Fe-sulfide (dominantly pyrrhotite) minerals.

The mineral textural characteristics of both samples at the micro scale fall into a liberation-dominated textural regime (Fe-sulfide liberation > 70% and grain size $I_{50} > 15\mu\text{m}$), which is consistent with the static characterisation tests providing an indication of the ‘worst point scenario’ of ARD generation. Quantification of these liberation characteristics, however, did not change the overall interpretation of

the characterisation test results but rather provided more certainty and accuracy to the waste rock classification.

Kinetic prediction (humidity cell) test results remained circumneutral in pH over 52 weeks, showing an absence of acidic leachate formation. Only minor Fe-sulfide dissolution occurred despite the relatively high grades of Fe-sulfide minerals (8.6% and 31% for samples B and C, respectively). The lack of acidic leachate generation was attributed to a combination of the following mineral texture factors: both samples, in addition to Fe-sulfide minerals, contained carbonate (dissolving) minerals (2.2% and 13% for samples B and C, respectively), which had the potential to neutralise some of the acidity formed in the cells over the 52 weeks; over 50% of the Fe-sulfides in the sample occurred in the +1mm size fractions that showed negligible liberation (surface exposure), resulting in a net Fe-sulfide liberation for the sample of 14% and 25% for samples B and C, respectively; overall carbonate mineral liberation was similarly low (between 11 and 16%); unliberated Fe-sulfide and carbonate (dissolving) minerals in both samples showed strong associations to intermediate weathering, slow weathering and inert minerals.

The mineral textural characteristics of both samples on the meso scale (> 1mm) fell into an association (locking) dominated textural regime due to the high degree of Fe-sulfide encapsulation. Measurement of Fe-sulfide grain size distributions similarly supported these findings (grain size d_{90} being 210 μ m and 550 μ m for samples B and C, respectively). Quantification of the liberation characteristics on a particle size-by-size basis was critical to the interpretation of the test results and provided more certainty and accuracy to the prediction of the ARD potential of the waste material.

A combination of the results from both the micro scale (static) characterisation tests and meso scale characterisation and prediction tests (humidity cell) alongside quantitative mineral-textural analyses was central to the development of a more complete understanding of the ARD generating characteristics of the waste rock material. This provides more certainty and accuracy to waste rock classification and modelling of the long term ARD generating properties. This in turn allows site specific predictions of the long term impacts thus ultimately guiding the necessary interventions required.

This work has developed an African case study (comprising both a pyrite and pyrrhotite waste rock sample) to recommend that mineral textural information is a critical component of the ARD characterisation and prediction testing protocol and that its integration into standard international testing protocol is required. Alongside the African case study, three additional independent case studies have been highlighted in the literature representing waste rock studies from Canada, Australia and Scandinavia spanning a variety of waste rock types (including differing mineralogy and texture), and climate. Collectively these four case studies provide a strong evidence base on which the international agency can be approached.

The following recommendations are made:

- Quantification of mineral grades (also known as bulk mineralogy or modal abundance) is required as part of the static ARD characterisation testing protocol since the information provides certainty to waste rock classification. Quantitative mineral texture measurements of this material provide additional information accompanying the static characterisation tests (particularly if the application of a liberation correction is desired), but this represents supporting information rather than required information;
- Quantification of (i) mineral grades (also known as bulk mineralogy or modal abundance), (ii) mineral grade on a particle size-by-size basis (also known as mineral distribution by size) and (iii) sulfide and carbonate mineral liberation and association on a particle size-by-size basis is required as part of humidity cell testing protocol;
- The results of this study are collectively collated with those of three other published international case studies as a representative and strong evidence base to recommend the prescription of

mineral textural information into the larger context of South African and global protocol on ARD characterisation and prediction.

Acknowledgements

The research team in this project gratefully acknowledges the support of the WRC for this project. Further, the SARChI Research Chair Initiative has contributed through the support of related and complementary research through the Chairs in Mineral Beneficiation and Bioprocess Engineering (held by Profs Jochen Petersen and Sue Harrison). Technical support from Lorraine Nkemba, Gaynor Yorath, Keshree Pillay, Shireen Govender, Kenneth Maseko, Monde Bekaphi, Emmanuel Ngoma and Tichaona Samkange – all within the Department of Chemical Engineering – is also gratefully acknowledged with respect to assistance in sample preparation, mineralogical analyses and set-up of the laboratory testing. Dr Agnes Odri is also thanked for her continued sampling of sample C humidity cells in 2019, as well as Lesley Mostert for final proofing of this document.

The encouragement and support of the late Prof Dee Bradshaw (former Direction of the Minerals to Metals Initiative) on this project is fondly remembered.

Selected results reported in this work are sourced from the on-going PhD study of Mr Alex Opitz (funded through the Minerals to Metals Initiative at the University of Cape Town). All material derived from the PhD study of Mr Opitz will be referenced accordingly.

Guidance from the reference group, particularly through the leadership of Mr Yazeed van Wyk, is also acknowledged.

Reference Group

Mr Yazeed van Wyk
Dr Lore-Mari Deysel
Mr Graham Trusler
Dr Glen Nwaila
Ms Carla Hudson
Mr Nkateko Kubayi

Affiliation

Water Research Commission
University of the Free State
Digby Wells Environmental
University of the Witwatersrand
Mine Water Coordinating Body
Water Research Commission

Research Team

A/Prof Megan Becker
Miss Olga Guseva
Mr Alexander K.B. Opitz
A/Prof Jennifer L. Broadhurst
Prof Susan T.L. Harrison

Role

Project Leader
MSc Candidate
PhD Candidate
Academic collaborator
Academic collaborator

Table of Contents

Research Highlights	i
Executive Summary	iii
Acknowledgements	v
Table of Contents	vii
List of figures	ix
List of tables	xi
Acronyms and abbreviations	xiii
Glossary of terms	xv
1 Introduction	1
1.1 Problem Statement	1
1.2 Objectives	2
2 Acid Rock Drainage in Context	3
2.1 The chemistry of acid rock drainage formation	3
2.1.1 Acid formation	3
2.1.2 Acid neutralisation	4
2.2 The significance of mineral texture	5
2.2.1 Textural parameters: particle size, liberation, grain size distribution and morphology	6
2.3 Current acid rock drainage assessment strategies	8
3 ARD characterisation on the micro scale	11
3.1 Samples and sample preparation	11
3.2 Mineralogy and texture	11
3.2.1 Experimental method	11
3.2.2 Bulk mineralogy	12
3.2.3 Fe-sulfide liberation, association and grain size distribution	14
3.3 Characterisation tests	15
3.3.1 Geochemical static tests	15
3.3.2 UCT biokinetic test	18
4 ARD characterisation and prediction on the meso scale	23
4.1 Samples and sample preparation	23
4.2 Mineralogy and texture	24
4.2.1 Experimental method	25
4.2.2 Bulk mineralogy	26
4.2.3 Fe-sulfide liberation, association and grain size distribution	27
4.2.4 Dissolving mineral liberation, association and grain size distribution	30
4.3 Humidity cell tests	31
4.3.1 Experimental method	32
4.3.2 Sample characterisation	32
5 The importance of mineralogy and texture in the ARD assessment “toolbox”	37
5.1 Synthesis of micro and meso scale ARD characterisation and prediction test results	37
5.2 Importance of mineralogy and texture on the interpretation of ARD prediction test results	38
5.3 A case study to support the recommendation for the integration of mineral textural information into the larger context of global protocol on ARD characterisation and prediction	40
6 Conclusions	43
6.1 Quantification of the effect of mineral texture on ARD characterisation at the micro scale	43
6.2 Quantification of the effect of mineral texture on ARD characterisation and prediction at the meso scale	44
6.3 Integrating quantitative mineral texture measurements into the ARD characterisation protocol for improved accuracy in ARD characterisation and prediction	44
6.4 Recommendations	45
References	47
Supplementary content	53

List of Figures

Figure 2-1	Illustration of pyrite (Py) on the meso and micro scales. Qtz = quartz; Vc = volcanic rock. Images from Parbhakar-Fox (2012).....	6
Figure 2-2	Diagram showing the difference between particles, minerals and grains	7
Figure 2-3	Diagrammatic representation of mineral liberation	7
Figure 3-1	FEG QEMSCAN microscope.....	12
Figure 3-2	Polished sample blocks	12
Figure 3-3	Bulk mineralogy of sample B and C (QEMSCAN) represented in terms of weathering rates	13
Figure 3-4	Fe-sulfide liberation and association for samples B and C (QEMSCAN). The association describes the interrelationship of unliberated Fe-sulfide mineral grains with other minerals present in the waste rock sample. These data correspond to those presented in Table 3-2	14
Figure 3-5	Fe-sulfide grain size distribution (GSD) for samples B and C (QEMSCAN). The I_{50} describes the size at which 50% of the Fe-sulfide grains are smaller than this size, while the I_{90} describes the size at which 90% of the Fe-sulfide grains are smaller than this size.....	15
Figure 3-6	Images from left to right illustrate the ANC test after heating of the solutions, the NAG test prior to 24 hours of reaction with peroxide, NAG test during boiling step, titration set-up for both ANC and NAG tests.....	17
Figure 3-7	Graphical representation of acid rock drainage potentials for samples B and C (classification plot after Stewart et al. (2006)	18
Figure 3-8	Diagrammatic representation of the oxidation of pyrite by iron-oxidising (FOB) and sulfur-oxidising (SOB) bacteria (adapted from Bryan, 2006)	18
Figure 3-9	UCT batch biokinetic test experimental set-up	20
Figure 3-10	UCT batch biokinetic test pH profile. pH-control limit line represents the pH to which the experimental flasks were adjusted each day, with the rise in pH attributed to the presence of neutralising minerals. The error reported is that obtained from 1x the standard deviation, which indicates the variation between the triplicate samples used in the test.....	21
Figure 3-11	UCT batch biokinetic test redox profile. The error reported is that obtained from 1x the standard deviation, which indicates the variation between the triplicate samples used in the test.....	22
Figure 4-1	Particle size distribution for the HCT feed material of samples B and C.....	23
Figure 4-2	Images from left to right: 70x70mm rough rock sample block holder with sample block; 70x70mm rough rock sample block; standard and vertical section sample blocks (30mm diameter)	25
Figure 4-3	Mineralogy by particle size fraction as well as the reconstituted bulk mineralogy of the HCT feed for samples B and C	26
Figure 4-4	Mineralogy by particle size fraction as well as the reconstituted bulk mineralogy of the HCT feed for samples B and C, with a 100% indicating the full sample mass	27
Figure 4-5	Fe-sulfide liberation and association for samples B and C (QEMSCAN). The association describes the interrelationship of unliberated Fe-sulfide mineral grains with other minerals present in the waste rock sample. These data correspond to those presented in Table 4-2	27
Figure 4-6	Unsize Fe-sulfide mineral grain size distribution for meso scale samples B (n=52273) and C (n=60897) where n is the total number of dissolving mineral-bearing particles analysed	29
Figure 4-7	False-colour images of the Fe-sulfide-bearing particles in samples B (a) and C (b). See Figure 4-5 for colour legend.....	30
Figure 4-8	Dissolving mineral liberation and association for samples B (n=81804) and C (n=146442) (QEMSCAN), where n is the total number of dissolving mineral-bearing particles analysed. The association describes the interrelationship of unliberated dissolving mineral grains with other minerals present in the waste rock sample.....	30

Figure 4-9	Unsize dissolving mineral grain size distribution for meso scale samples B (n=81804) and C (n=75011) where n is the total number of dissolving mineral-bearing particles analysed	31
Figure 4-10	Humidity cell test set up.....	32
Figure 4-11	Water-fed humidity cell test pH profiles for samples B and C over the duration of 52 weeks. Data for sample B is sourced from the ongoing work of Opitz et al. (unpublished). The error reported is that obtained from 1x the standard deviation, which indicates the variation between the duplicate samples used in the test	33
Figure 4-12	Water-fed humidity cell test redox potential profiles for samples B and C over the duration of 52 weeks. Data for sample B is sourced from the ongoing work of Opitz et al. (unpublished). The error reported is that obtained from 1x the standard deviation, which indicates the variation between the duplicate samples used in the test.....	33
Figure 4-13	Cumulative total iron and sulfate extraction over the 52-week HCT test period for water-fed samples B and C. Error bars indicate 1x the standard deviation between replicate samples, which indicates the variation in concentration between the two replicate columns. It should be noted that the iron concentrations for the experiments was below the detection limit of 0.01mg/L for the assay method used to assess the iron concentration (APHA, 1998). Errors in sulfur extraction values do not include the 12% error previously reported for the barium chloride sulfate assay (APHA, 1995; Moosa, 2000)	35
Figure 5-1	Summary of sample B and C characteristics, with arrows indicating the areas which they inform.....	38

List of Tables

Table 2-1	Neutralising minerals and their reactivity at pH 5 (Lawrence & Scheske (1997) and references therein, after Sverdrup (1990) and Kwong (1993))	5
Table 2-2	Summary of the more commonly practiced ARD assessment strategies (adapted from Parbhakar-Fox & Lottermoser (2015) – a more detailed summary of all available ARD assessment tests may be found in the same resource).....	9
Table 3-1	Bulk mineralogy (reported in wt.%) for samples B and C using QEMSCAN	13
Table 3-2	The mass % distribution of the total Fe-Sulfide in the sample between liberated (>90% area exposed) and unliberated (<90% area exposed) categories. n = number of Fe-sulfide-bearing particles analysed. Selected false colour QEMSCAN particle images are included for visualisation (see Fig 3-4 for colour legend)	15
Table 3-3	Results of acid rock drainage characterisation tests for samples B and C. MPA = maximum potential acidity; ANC = acid neutralising capacity; NAPP = net acid producing potential; NAG = net acid generation; PAF = potentially acid forming; UC = uncertain	17
Table 3-4	Optimal conditions for select mesothermal bacterial species present in waste rock dumps and those used in the UCT biokinetic test developed by Hesketh et al. (2010) (Schippers et al., 2014).....	19
Table 4-1	Measurement settings used during QEMSCAN operation for meso scale size fractions. FI = field image; PMA = particle mineralogical analysis	25
Table 4-2	The mass % distribution of the total Fe-Sulfide in the sample between liberated (>90% area exposed) and unliberated (<90% area exposed) categories. n = number of Fe-sulfide-bearing particles analysed	28
Table 5-1	Summary of the case study data base intended to be used to motivate for the inclusion of mineral-textural information into standard global practice.....	42
Table A-1	XRF data for samples B and C	53
Table A-2	Bulk mineralogy for samples B and C as determined using quantitative XRD.....	54
Table A-3	Sized mineralogy for samples B as determined using QEMSCAN	55
Table A-4	Sized mineralogy for samples C as determined using QEMSCAN	55
Table A-5	Distribution of iron across the minerals in samples B and C as a percentage of the total iron in the sample. This was obtained using the Electron Probe Microanalysis (EPMA) data sourced from Opitz et al. (2020) for sample B, and QEMSCAN mineralogy data for samples B and C.....	56
Table A-6	Minerals and corresponding chemical formulae	57

Acronyms and Abbreviations

ABA	Acid-base accounting
ANC	Acid neutralising capacity
AP	Acid potential
ARD	Acid rock drainage
ARDI	Acid rock drainage index
EPMA	Electron probe micro-analysis
GARD	Global acid rock drainage (guide)
GOF	Goodness of fit (statistical indicator associated with QXRD data)
GSD	Grain size distribution
HCT	Humidity cell test
ICP-MS	Inductively coupled plasma mass spectrometry
ICP-OES	Inductively coupled plasma optical emission spectrometry
INAP	International network for acid prevention
LA-ICP-MS	Laser ablation inductively coupled plasma mass spectrometry
MLA	Mineral liberation analyser
Mol	Mineral of interest
MPA	Maximum potential acidity
NAF	Non-acid forming
NAG	Net acid generation
NAPP	Net acid producing potential
NP	Neutralisation potential
NRF	National Research Foundation
PAF	Potentially acid forming
PSD	Particle size distribution
QEMSCAN	Quantitative Evaluation of Minerals by Scanning Electron Microscopy
QXRD	Quantitative X-ray diffraction
Rwp	R-weighted pattern (statistical indicator associated with QXRD data)
SARChI	South African Research Chairs Initiative
SEM-EDS	Scanning electron microscopy with energy dispersive spectrometry
SIP	Species identification protocol
UC	Uncertain
UCT	University of Cape Town
XCT	X-ray computed tomography
XRD	X-ray diffraction
XRF	X-ray fluorescence

Glossary of Terms

Association	Quantified perimeter association between two mineral phases
Dissolving	Relative reactivity of a neutralising mineral at pH 5 (see Table 2-1)
Fast weathering	Relative reactivity of a neutralising mineral at pH 5 (see Table 2-1)
Fe-sulfide	Pyrite and / or pyrrhotite
Grain	A three-dimensional fragment consisting of only one mineral
Inert	Relative reactivity of a neutralising mineral at pH 5 (see Table 2-1)
Intermediate weathering	Relative reactivity of a neutralising mineral at pH 5 (see Table 2-1)
Liberated	A particle comprising greater than 90% by area of the mineral of interest
Liberation	State of a particle consisting of only one phase
Locked	A particle comprising less than 30% by area of the mineral of interest
Locking	Description of the mineral association characteristics of an unliberated mineral of interest
Middling	A particle comprising between 30% and 90% by area of the mineral of interest
Particle	A three-dimensional fragment consisting of one or more mineral phases
Slow weathering	Relative reactivity of a neutralising mineral at pH 5 (see Table 2-1)

1 Introduction

1.1 Problem Statement

Today more than ever, minerals and metals play a critical role in our modern society, particularly since it has been recognised that mining is a key enabler in meeting the United Nations' Sustainable Development Goals (Columbia Center on Sustainable Investment et al., 2016). Mining, mineral processing and metallurgy however, are not waste-free processes. The majority of the mined material ultimately finds its way into massive heaps or dumps, and as the need for metals increases with increasing population and urbanisation, larger volumes of lower grade material are excavated to produce more waste rock. The generation of mine wastes, in most cases, is accompanied by a host of negative environmental side effects, one of these being acid rock drainage (ARD). This phenomenon results in acidified waters with high sulfate concentrations and elevated levels of deleterious elements, making this water unfit for human consumption and destructive to the surrounding fauna and flora.

ARD occurs through the combined effects of acid formation and neutralisation reactions, specifically through the oxidation of metal sulfides, dissolution of gangue minerals (such as various carbonate and silicate minerals) and release of deleterious metals into freshwater systems. The naturally occurring phenomenon initially proceeds through sulfide mineral oxidation upon exposure to atmospheric oxygen and water. This reaction is exacerbated by mining activities, which fragment the parent rock into material that has an exponentially larger surface area available to oxidative conditions (INAP, 2009; Jamieson et al., 2015; McCarthy, 2011; Morin & Hutt, 2001). Iron sulfide minerals such as pyrite and pyrrhotite are often found in base and precious metal ores and because of their relative abundance they are typically recognised as the main acid forming minerals in mine wastes; however, all mineral sulfides are susceptible to oxidation (Nordstrom & Alpers, 1999; INAP, 2009). Carbonate (calcite, dolomite and magnesite) and some silicate minerals have the potential to consume the acid formed through sulfur-bearing mineral oxidation, affecting both the pH and the ionic content of the drainage waters (Plumlee, 1999). In addition to mineralogy, the type of oxidant, pH, climatic conditions and the presence of naturally occurring acidophilic bacteria affects the rate of ARD formation (Akcil & Koldas, 2006).

The ARD potential of waste rock and tailings material may be assessed in various ways, more commonly using standard ARD characterisation and prediction practices, which consist of a series of geochemical static and kinetic tests (Smart et al., 2002). The former generally comprises acid-base accounting (ABA) and net acid generation (NAG) tests, which provide an indication of the extremes of acid formation and neutralisation potentials with no indication of the relative rates of these reactions. These tests can be performed on many samples quickly and at a relatively low cost (INAP, 2009). Kinetic tests, such as the commonly used humidity cell test (HCT), aim to assess the lag time for acid formation, the reaction rates, and the change in leachate quality with time (White et al., 1997). These are very time-consuming, running for a minimum of 20 weeks (Smart et al., 2002), up to 60 weeks (Brough et al., 2013) or longer. The University of Cape Town (UCT) biokinetic test (Hesketh et al., 2010; Golela et al., 2018; Makaula et al., 2018) was developed to address the catalysing effects of acidophilic bacteria, providing a methodology for assessing reaction rates of key minerals involved in acid formation and neutralisation in the presence of microbes.

In some cases these tests may fail to adequately characterise and predict the ARD potential of mining wastes due to the inherent complexity of the mechanisms associated with ARD formation and an incomplete understanding of all the governing factors. Several authors (Becker et al., 2015; Brough et al., 2013; Dyantyi et al., 2013; Morin & Hutt, 1998; Paktunc, 1999; Parbhakar-Fox et al., 2011) have argued that this is due to mineral texture being a critical parameter in controlling ARD generation (both in small scale characterisation and prediction methodologies, and on the larger field scale). In mineralogy and geology, texture is defined as the interrelationship of different mineral grains with one another as well as their shapes and sizes (Becker et al., 2016). Textural parameters include the

exposure of acid forming and acid neutralising minerals to the atmosphere (liberation), their association with other minerals, their grain size distribution and shape (Parbhakar-Fox et al., 2011). The understanding, quantification and interpretation of these parameters is essential to facilitate the understanding and enhancement of existing test methods, as a poor understanding of the role of texture on ARD generation can ultimately lead into either over engineering or under engineering for ARD prevention and mitigation, both of which have significant techno-economic, environmental and social consequences (Jennings and Dollhopf, 1995). Historically the lack of focus in this area has been due to (i) the sheer scientific complexity of quantitative mineral textural descriptors, (ii) the limitations of analytical technology for quantitative textural measurements, (iii) the high costs associated with running these measurements to get statistically representative and accurate data, and (iv) that current accepted international and local protocol for ARD characterisation and prediction (e.g. Global Acid Rock Drainage Guide, American Standard Test Methods, DWARF, 2008) not necessitating quantitative textural measurements, but rather recommending them, with little guidance on the specifications of how they should be conducted. Furthermore, the real economic value of automated mineralogy techniques is still not fully recognised even in the context of valuable mineral beneficiation (Gu et al., 2014). In the last two decades, however, there have been significant positive developments in mineral textural quantification coming out of the mineral processing and extractive metallurgy industries that are of direct relevance to ARD characterisation. This includes the development of new analytical technology (e.g. automated scanning electron microscope with energy dispersive spectrometry (SEM-EDS) for quantitative mineralogy and X-ray computed micro-tomography), and new textural descriptors (e.g. Pérez-Barnuevo et al., 2013; Vos, 2017; Jardine et al., 2018).

These advances provide an ideal opportunity to integrate textural and mineralogical techniques into the ARD assessment toolbox and address the necessity for relevant and practical protocols for meaningful and accurate ARD characterisation and prediction. This will help mitigate and prevent the generation of ARD from mining activities, and the subsequent contamination of the associated water resources. The development of these protocols should be based on a sound understanding of the various chemical reactions taking place on a mineral particle scale and the respective reaction rates, which are ultimately a function of the accessibility of oxygen and water to the different minerals and their texture. It is essential to develop a more sound understanding of the effect of mineral texture on the various ARD-forming and neutralising reactions taking place both at the small scale of laboratory static and kinetic tests, and also on the larger field scale (see also Brough et al., 2013; Parbhakar-Fox et al., 2013; Becker et al., 2015; Parbhakar-Fox & Lottermoser, 2015; Opitz et al., 2016a).

1.2 Objectives

The overarching objective of this project is to quantitatively evaluate the role of mineralogy and texture in the context of commonly practiced ARD characterisation and prediction tests on both fine (micro scale) and coarse (meso scale) material. This objective can be further broken down into discrete project aims as follows:

- (d) To quantify the effect of mineral texture on ARD characterisation on the micro scale (specifically in the context of small-scale laboratory static and biokinetic tests).
- (e) To quantify the effect of mineral texture on ARD characterisation on the meso scale (specifically in the context of small-scale laboratory kinetic tests).
- (f) To develop the case study supporting a recommendation to prescribe integration of mineral textural information into the larger context of global protocol on ARD characterisation and prediction.

Each of the abovementioned objectives is addressed in a dedicated chapter of this report.

2 Acid Rock Drainage in Context

Overview: This chapter provides a review of the relevant literature relating to the formation of acid rock drainage, the role of mineral texture, and reviews current practice in the characterisation and prediction of acid rock drainage (ARD).

2.1 The chemistry of acid rock drainage formation

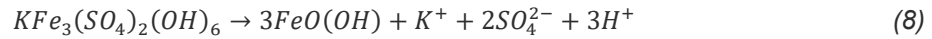
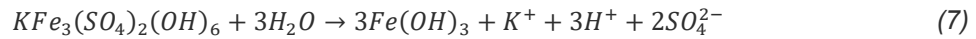
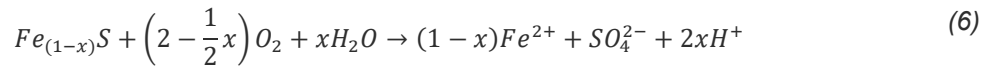
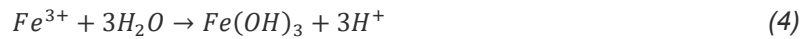
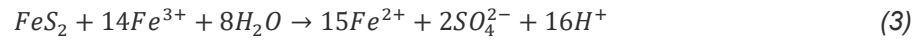
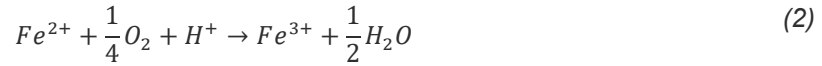
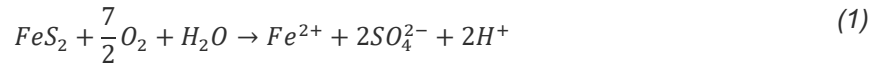
Acid rock drainage (ARD) forms through a complex series of acid formation and neutralisation reactions at both active and abandoned mining sites. The naturally occurring phenomenon is associated with both waste rock and tailings primarily from the mining of coal, gold, copper, nickel, and lead-zinc (Nordstrom & Alpers, 1999; Akcil & Koldas, 2006). Accelerated by microbial effects, the oxidation of sulfur-bearing minerals in the waste material leads to acid formation, while acid neutralisation is a result of the dissolution of carbonate minerals, as well as some of the more reactive fast and intermediate weathering silicate minerals (Becker et al., 2015; INAP, 2009). The resulting drainage waters are termed ARD and are characterised by neutral to low pH, high salinity, and elevated levels of deleterious elements (INAP, 2009). Many factors affect the rate of formation of ARD. These include the mineralogy, pH, type of oxidant (oxygen or ferric iron) and its concentration, mineral texture and morphology (mineral shape and structure) and the presence and respective amounts of trace elements (Akcil & Koldas, 2006). The dissolution of various minerals facilitates the ARD formation process. These may be either the primary minerals present originally in the rock or secondary minerals originating from the dissolution of primary minerals. A comprehensive summary of primary and secondary minerals involved in ARD generation may be found in Plumlee (1999), Morin & Hutt (2001) and Jamieson et al. (2015), with a summary of all minerals mentioned in this report being provided in alongside their respective chemical formulae in Supplementary Content, Table A-6. The geochemistry of ARD formation is inherently complex and has been reviewed in greater detail outside this report (Nordstrom and Alpers, 1999; Plumlee, 1999; Lottermoser, 2010). A brief overview of acid formation and neutralisation is however provided in sections 2.1.1 and 2.1.2.

2.1.1 Acid formation

Lapakko (2002) outlined three main pathways for the formation of acid in mine wastes, namely the oxidation of iron sulfides, dissolution of alunite and jarosite, and the dissolution of soluble sulfates. The main sulfide minerals contributing to acid formation are pyrite, marcasite and pyrrhotite (Plumlee, 1999). The dissolution of soluble sulfates, as outlined by Lapakko (2002), that may lead to acid formation refers to minerals such as melanterite, romerite, copiapite, rozenite and szomolnokite, which are soluble hydrated iron-sulfate minerals occurring as efflorescent salts on weathered pyrite surfaces. These minerals provide an additional and rapid source of acidity, particularly in very wet environments (rain season) and play a role in the lag phase of ARD formation. Additionally, jarosite formed as a product of the weathering of primary acid forming minerals (such as pyrite and pyrrhotite) may either react with water or transform to the more stable iron oxide or hydroxide phase, releasing additional acidity.

Equations (1) to (5) show the reactions associated with pyrite, the main acid generating mineral in waste rock. Equation (1) represents the initial reaction followed by the oxidation of ferrous to ferric iron in equation (2). Reaction (3) occurs at pH 4.5, where ferric iron becomes the primary oxidizing agent. Decreasing the pH value to between 3 and 4.5 yields reactions (4) and (5) with the precipitation of $\text{Fe}(\text{OH})_3$ and FeOOH (Lapakko, 2002; Parbhakar-Fox & Lottermoser, 2015). The simplest form of the pyrrhotite oxidation reaction is presented in equation (6) (Moncur et al., 2009).

The reactions of jarosite generating acidity are shown in equations (7) and (8) below, with the latter representing the reaction of jarosite to goethite (White et al., 1997).



2.1.2 Acid neutralisation

Of foremost importance for acid neutralisation are the primary neutralising minerals. These include, in the order of decreasing dissolution rate, calcite, dolomite, magnesite and ankerite. Manganese and iron carbonates (rhodochrosite or siderite) do not contribute to neutralisation potential because although they provide initial neutralisation upon dissolution, they do not contribute to net neutralising capacity in waste rock, as they may re-precipitate to release acid (Lapakko, 2002). The two possible pathways for calcite dissolution are shown in equations (9) and (10) below, which represent the dominant calcite reactions for pH above and below 6.4, respectively.



Magnesium- and calcium-bearing end members of fast, intermediate and slow weathering silicate minerals (such as those listed in Table 2-1) and some slow weathering silicates such as chlorite and mica, may also offer long-term acid-buffering capacity (Jambor et al., 2007; Becker et al., 2015). Some examples of how this happens are shown in the acid neutralising reactions of anorthite (11) and forsterite (12). Additionally, Lapakko et al. (2006) showed that below pH 6 magnesium- and calcium-bearing silicates contribute to the acid buffering capacity in a humidity cell test set-up.



Overall, the relative rates of dissolution show an inverse relation to the Bowen's reaction series and the order of mineral crystallisation (Bowen, 1922). The relative reactivity and dissolution/weathering potential of various minerals at pH 5 was represented by Lawrence & Scheske (1997) and is provided in Table 2-1.

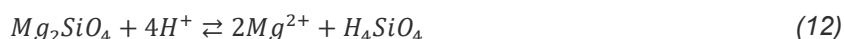


Table 2-1 Neutralising minerals and their reactivity at pH 5 (Lawrence & Scheske (1997) and references therein, after Sverdrup (1990) and Kwong (1993))

Reactivity at pH 5		Typical minerals
Dissolving	1.00	Carbonates (calcite, aragonite, dolomite, magnesite, brucite)
Fast weathering	0.40	Feldspar (anorthite), olivine (forsterite), pyroxenes (diopside, hedenbergite, jadeite, spodumene, bronzite), wollastonite, garnets, epidotes, nepheline, leucite
Intermediate weathering	0.02	Pyroxenes (enstatite, augite), amphiboles (tremolite, actinolite, hornblende, glaucophane, anthophyllite), serpentine (chrysotile), mica (biotite), chlorite, talc, hypersthene
Slow weathering	0.01	Feldspar (albite, oligoclase, labradorite), clay (kaolinite, vermiculite, montmorillonite)
Very slow weathering	0.01	Feldspar (K-feldspar), mica (muscovite)
Inert	0.004	Rutile, zircon, quartz, sphene

2.2 The significance of mineral texture

Mineral texture describes the interrelationship of the individual mineral grains comprising a rock, their grain size distribution, as well as their respective sizes and shapes (Becker et al., 2016). Textural factors influencing the generation of ARD include the degree of liberation of minerals of interest (acid forming and neutralising minerals) and their grain size distribution, mineral associations, reactivity and the available reactive surface areas (Parbhakar-Fox et al., 2011).

Three general scales of texture classification can be used, namely the macro, meso and micro texture. The macro scale provides information regarding the overall texture without specific information about the location of individual grains and can be considered on the scale of an outcrop. Meso texture is used to describe the information regarding the grain and phase boundaries, while the micro texture involves analyses of the individual mineral grains and their orientations (Strotzki, 2010). An alternative way of interpreting meso and micro texture may be that the former can be seen with the naked eye, while the latter would require optical or electron microscopy to discern. The acid rock drainage index (ARDI) developed by Parbhakar-Fox et al. (2011) provides an excellent illustration of the role and need for textural quantification on the meso and micro scales to better predict ARD generation. An indication of the differences observed on the micro and meso scale is provided in Figure 2-1.

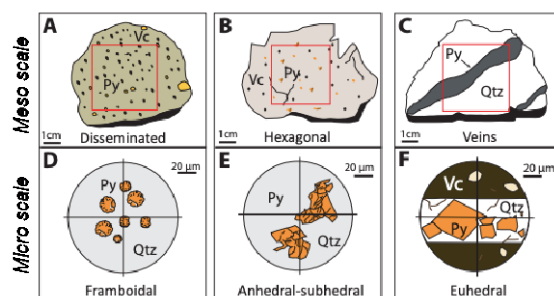


Figure 2-1 Illustration of pyrite (Py) on the meso and micro scales. Qtz = quartz; Vc = volcanic rock. Images from Parbhakar-Fox (2012)

Although texture and mineralogy have been only little studied in the ARD context, much of the pioneering work in quantitatively describing mineral textures has evolved from mineral processing and metallurgical studies. Alongside this has been the development of custom built analytical technology using the automated scanning electron microscope with energy dispersive spectrometry (SEM-EDS) to quantitatively measure textural parameters such as liberation and grain size distribution from 2D sections (Gay, 2004; Leigh et al., 1993; Wightman & Evans, 2014). Some of the more well-known instruments with this functionality include the QEMSCAN (Quantitative Evaluation of Minerals by Scanning Electron Microscopy), MLA (Mineral Liberation Analyser), TIMA (TESCAN integrated mineral analyser) and Mineralogic instruments. More recent advances in analytical technology may allow users the opportunity to image and quantify mineral texture in 3D using X-ray computed micro tomography (Miller et al., 2009; Elghali et al., 2018, 2019). Furthermore, in hydrometallurgical processes (such as chemical- or bioleaching) textural factors such as liberation, particle size, porosity, reactive surface area and mineral associations have previously been studied due to their influences on the recovery of valuable metals. It is assumed that the mechanisms dominant in heap leach systems are similar to those present during ARD formation, which include effects of acidophilic bacteria, mineralogy, particle size, mineral liberation, association and weathering, as well as galvanic interactions between sulfide phases. Although heap leaching processes make use of coarser size fractions than those used for common ARD tests (12-25mm vs. 6.3mm and finer top size for heap leaching and ARD testing, respectively), these dominating mechanisms may still be investigated, even though the results of heap leach tests are not directly comparable to the results obtained via ARD testing. The drawing of parallels between hydrometallurgy and ARD generation is important for improved understanding of ARD formation.

The necessity for the incorporation of textural and mineralogical analyses into ARD methodologies is shown through several case studies outlined by Brough et al. (2013, 2018) and Elghali et al. (2018, 2019). These demonstrate that results obtained solely via commonly used ARD assessment techniques may be misinterpreted if inadequate consideration is given for sulfide mineralogy and texture, as well as the possible neutralisation contributions from various neutralising minerals and their weathering products. Misinterpretation of results and therefore over- or underestimation of ARD potential on site could have financial implications for mine start-up or, alternatively, devastating environmental effects.

2.2.1 Textural parameters: particle size, liberation, grain size distribution and morphology

A particle is a three-dimensional fragment consisting of one or more mineral phases (see Figure 2-2). Naturally, the particles within a sample are mostly of irregular size and therefore precise size measurement is unobtainable on a large scale. A particle size distribution (PSD) is used to define the continuous size distribution of particles within a certain range and is commonly obtained via sieving or screening techniques that provide a PSD irrespective of the particle shape (Mainza & Powell, 2016).

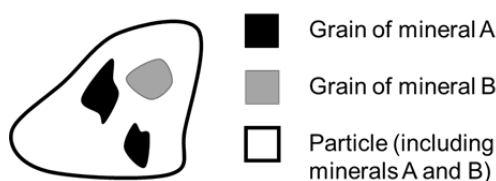


Figure 2-2 Diagram showing the difference between particles, minerals and grains

Liberation is the state of a particle consisting of only one phase. Particles containing multiple minerals can be termed as “unliberated, locked or composite”. A diagrammatic representation of liberated and unliberated particles is presented in Figure 2-3. This is important when considering the results of SEM analyses, as particles that have even a single pixel of an alternative mineral in the image section will be classified as unliberated. Liberated material is therefore rarely defined as that which is 100% liberated, but rather using a slightly lower number (80% or 90% are more common cut-off points). Acid-forming and neutralising minerals may be liberated or unliberated (composite) and be present as inclusions in other minerals. This directly affects the available reactive surface area of the mineral (Evans & Morrison, 2016). Acid forming and neutralising minerals present as inclusions in inert materials, such as quartz, will be unavailable for reaction. Alternatively, defects in the particle, such as cracks or fractures, have the potential to increase the reactive surface area of minerals, and consequently increase their potential for reactivity (Lapakko, 2002).

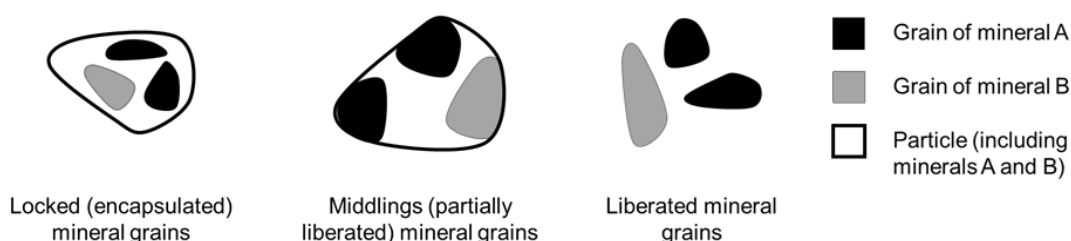


Figure 2-3 Diagrammatic representation of mineral liberation

For humidity cell tests liberated material has been found to be more likely to produce acidic leachate than material with a lower degree of liberation (Brough et al., 2017; Elghali et al., 2019). This phenomenon is also well described in heap bioleaching studies (Fagan-Endres et al., 2017). Sulfide morphology also affects available reactive surface area. Framboidal or euhedral morphology in pyrite will affect the reactive surface area, with the former having a larger reactive surface area resembling that of a raspberry (with framboidal originating from the French word *framboise*, meaning raspberry) and therefore having a higher reactivity. Euhedral pyrite has a flat surface and therefore a smaller reactive surface area (Weber et al., 2004).

Another textural factor related to mineral liberation and influencing ARD formation is the grain size of acid forming and neutralising minerals (Lapakko, 2002). The grain size refers to the size of a specific mineral within a particle of a specified size. Leaching process optimisation requires quantitative knowledge of the mineral grain size distributions, as the size and reactivity of individual mineral grains will affect the overall leach kinetics of the heap (Ghorbani et al., 2011). Fine sized, fully liberated particles have been shown to have an increased reactivity potential when compared to coarser particles containing encapsulated material (Fagan-Endres et al., 2017; Ghorbani et al., 2011).

Galvanic interactions, which occur through the association of sulfides with one another, play a considerable role in the rates of sulfide oxidation. This phenomenon is the preferential reactivity of certain sulfide phases over other contacting sulfide phases due to a difference in their standard electrode potentials. Ghorbani et al. (2013) and INAP (2009) outlined that galvanic interactions have a significant effect on the leaching of sulfides present in a galvanic cell, with the extent of leaching

dependent on the relationship between the electrostatic potentials between the sulfides. The electrostatic potentials of pyrite, chalcopyrite, sphalerite, pyrrhotite and galena decrease in this order (Kocabag, 1985) with pyrrhotite, galena and sphalerite exhibiting preferential oxidation over pyrite (when these minerals are in contact) due to their lower standard electrode potentials (INAP, 2009).

2.3 Current acid rock drainage assessment strategies

The research into effective ARD characterisation and prediction has been ongoing for decades, but prominent strides have been made in the last 20 years. With the problem of accurate ARD assessment persistent today, it is possible to conclude that the practices best at the time (several decades ago) would not characterise mine wastes efficiently due to incomplete knowledge of the mechanisms governing the ARD formation processes (INAP, 2009). Consequently, ARD remediation costs are high. As an example, the combined costs for ARD treatment of four of the world's largest mining countries (Canada, Australia, USA and South Africa) were predicted to be around US\$32-72 billion in 2018 (Cozzolino et al., 2018). This underlines the necessity for incorporating ARD prediction into the earliest stages of mine development and throughout the lifetime of the mine, as well as after mine closure (Parbhakar-Fox & Lottermoser, 2015). The numerous governing factors in ARD formation make the characterisation and prediction process a multidimensional problem. Although many tests and techniques are used, only a select subset are included in the commonly used test suite, with the selected set exhibiting regional variability based on local regulations and requirements (INAP, 2009). Table 2-2 provides an overview of the more commonly utilised ARD assessment practices, while a more comprehensive summary of the majority of existing tests may be found in Parbhakar-Fox & Lottermoser (2015).



Table 2-2 Summary of the more commonly practiced ARD assessment strategies (adapted from Parbhakar-Fox & Lottermoser (2015) – a more detailed summary of all available ARD assessment tests may be found in the same resource)

Technique	Test	Principle	Description	Advantages	Limitations
Static tests	ABA	Calculation of Net-Acid Producing Potential (NAPP = MPA-ANC)	MPA calculated from total sulfur ANC determined by laboratory titration methods	Industry-wide practice, with commercial laboratories offering this testing, therefore results are easy to understand and interpret	MPA overestimated if based on total S MPA and ANC tests are not performed on exactly the same sample material ABA procedure is not standardised, site-by-site comparisons are not possible
	Net acid generation (NAG) test	Determination of acid forming potential	Addition of hydrogen peroxide	Industry-wide practice NAG pH vs. NAPP geochemical plots are routinely used for waste classification	Hydrogen peroxide quality must be insured Calcite and dolomite may react during the test, resulting in alkaline pH values
Kinetic tests	Humidity cell test	Mimics the weathering of waste rock material with leachate chemistry assessed	ASTM D5744 method	More realistic indication of leachable metals than short term tests Attempts to mimic climatic cycle	Reaction products may be removed during the rinse Equilibrium conditions not reached due to short contact times No integration of mineralogical and microtextural analyses
Mineralogical characterisation	Bulk mineralogy	Quantification of acid forming and neutralising minerals	XRD	Quantitative mineralogy Data can be used for MPA/ANC calculations	Expensive Detection limits Not possible to identify trace phases
	Mineral textures	Classification of intact mineralogy	Automated SEM-EDS (e.g. MLA, QEMSCAN, TIMA-X, Mineralogic)	Well-established data collection procedure Negligible error margin with offline post-processing available Ability to utilise data collected as part of other resource characterisation work	No guidelines for ARD-relevant data collection or processing Technically challenging Expensive 2D analysis of polished sections

3 ARD characterisation on the micro scale

Overview: This chapter focuses on addressing objective number one that seeks to quantify the effect of mineral texture on ARD characterisation at the micro scale (<1mm), specifically in the context of small-scale laboratory static and UCT batch biokinetic tests.

3.1 Samples and sample preparation

The samples used in this study were obtained from the waste rock material of an African orogenic gold deposit and are labelled as Sample B and Sample C respectively. Sample B consisted of material from a waste rock dump (116 kg), while sample C was received in the form of drill core (17 kg). The bulk samples were individually crushed to have greater than 90% of the material passing 6.7mm and a bulk particle size distribution (PSD) was obtained. The crushed sample was then thoroughly mixed to homogenise the material and split into sub-samples of up to 3.5 kilograms using a rotary sample divider. PSDs were obtained for the sub-samples as a means to troubleshoot the representativeness of the splitting process, as sampling errors were assumed to be of greater significance with increasing particle size (at the initial sub-sampling stages).

Sub-samples were then randomly selected for characterisation testing, milled and screened to pass through a 150µm screen. This material was then further split into smaller portions as required for the characterisation test suite (2g-7.5g) and mineralogical and textural analyses (2g-10g).

For the purposes of representativeness, the minimum representative sub-sample mass at a particle top size of 150µm was 0.45g according to Gy's safety line (Gy, 1979). The ANC and NAG tests required a sample mass of 2g and 2.5g, with the rotary sample divider being used to split off 10g sub-samples of the milled material to allow for five and four replicates per test, respectively.

3.2 Mineralogy and texture

3.2.1 Experimental method

The bulk mineralogy, liberation and association were quantified using a FEI QEMSCAN 650F instrument with two Bruker XFlash 6130 EDS detectors at the University of Cape Town (Figure 3-1 below). Samples for mineralogical analysis were prepared as 30mm diameter epoxy mounted and polished 2D sections (see Figure 3-2) on sized material for sample B (in a series of discrete size fractions) and unsized (bulk) material for sample C. The broader size fractions, such as the unsized bulk samples and the smallest sized fraction samples were prepared as vertical/transverse section blocks to avoid bias due to the settling of heavier particles.

The processing of the QEMSCAN data was done using the FEI iDiscover software, which converts both the backscatter electron (BSE) and X-ray information into pixels containing elemental information. These are then classified as minerals through a specially developed, and user defined 'species identification protocol' (SIP) file. The size of the pixel (resolution) is also user-defined, depending on the requirements of the measurements.

For the micro scale characterisation test material (passing 150µm), the pixel size was set to 3µm. The pixel data were then collected and categorised by the user into entries that represent minerals based on their elemental information. A composition and density were assigned to these minerals to allow for the translation of the two-dimensional cross-section images to volume and mass data. When determining the bulk mineralogy, two user defined mineral lists were created, one to illustrate the

dominating minerals and the other to represent dominating mineral weathering/reactivity groupings, based on Table 2-1. The liberation and association data were obtained from built-in categorisers in the iDiscover software for mineral liberation and association. The association data were normalised with respect to the portion of Fe-sulfide material that was unliberated, with liberation set nominally to include material that has 90% or more of its particle cross sectional area exposed to the surrounding environment (resin in the sample block).

Sub-samples from the milled material were also split for powder X-ray diffraction (XRD) analysis, (performed using a Bruker D8 Advance diffractometer with a LynxEye detector and CoK α radiation, with quantitative phase analysis performed using Rietveld refinement in the Topas 4.1 software) (Bruker AXS GmbH, 2008), and X-ray fluorescence (XRF) spectrometry (with Rh tube and natural element standards). The detection limit for mineral analysis in XRD is ~ 2 wt.%, and for element oxide analysis in XRF is 0.01 wt.%. The XRD and XRF results were used to validate the mineralogical results obtained using QEMSCAN (see Supplementary Content). Further details of the sample preparation procedure for sample B is provided in Opitz et al. (2016a).



Figure 3-1 FEG QEMSCAN microscope

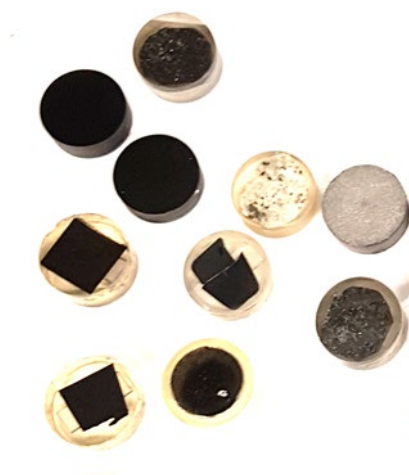


Figure 3-2 Polished sample blocks

3.2.2 Bulk mineralogy

Table 3-1 provides the bulk mineralogy of samples B and C obtained from QEMSCAN (for QXRD data, see Supplementary Content). The predominant minerals in sample B were quartz, plagioclase-feldspar (albite), mica (biotite/Fe-mica), Fe-oxide (magnetite), K-feldspar, Fe-sulfide (pyrite), carbonate (calcite), chlorite and amphibole (ferro-actinolite), while for sample C these were quartz, Fe-sulfide (pyrrhotite), carbonate (calcite), titanite, chlorite and K-feldspar.

Table 3-1 Bulk mineralogy (reported in wt.%) for samples B and C using QEMSCAN

Mineral	Sample B	Sample C
Pyrite	7.7%	2.0%
Pyrrhotite	<1%	29.2%
Carbonate	2.2%	12.5%
Epidote	<1%	<1%
Pyroxene	1.1%	<1%
Amphibole	3.8%	<1%
Mica	9.5%	7.6%
Chlorite	2.1%	4.7%
Talc	<1%	<1%
Plagioclase-Feldspar	21.3%	<1%
K-Feldspar	8.7%	5.3%
Fe-Oxide	10.6%	<1%
Quartz	30.8%	30.7%
Titanite	<1%	4.8%

The bulk mineralogy can be further represented in terms of the relative mineral weathering rates, as given in Figure 3-3 (see also Table 2-1). The Fe-sulfide grouping in sample B was dominated by pyrite and sample C by pyrrhotite. The dissolving mineral category in both samples was dominated by calcite, with sample C containing considerably more (12.5%) than sample B (2.2%). In addition to Fe-sulfide and dissolving mineral categories, the mineralogy for sample B was dominated by the slow weathering (21.3% plagioclase-feldspar, 10.6% Fe-Oxide (magnetite), 8.7% K-feldspar), inert (30.8% quartz) and intermediate weathering (9.5% Fe-mica, 2.1% chlorite) minerals, while sample C was dominated by inert (30.8% quartz, 4.8% titanite), followed by dissolving (12.5% calcite), intermediate weathering (7.6% Fe-mica, 4.7% chlorite), and slow weathering (5.3% K-feldspar) minerals.

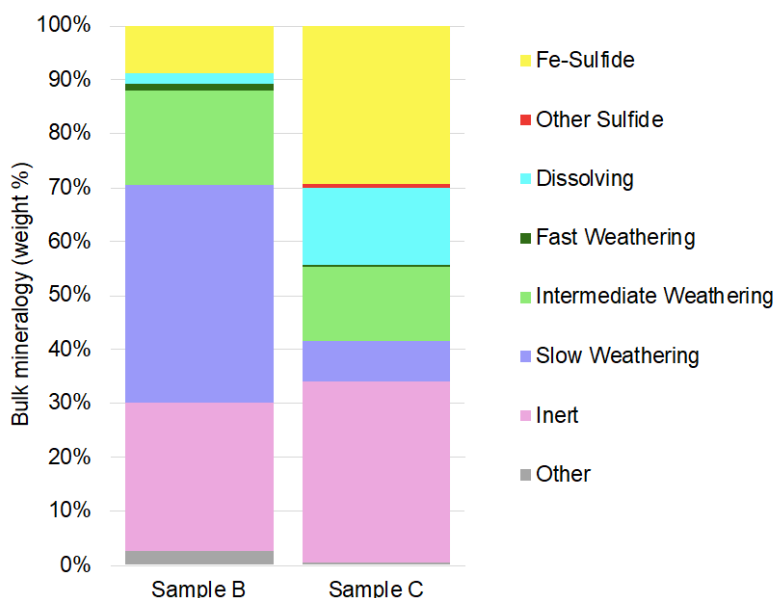


Figure 3-3 Bulk mineralogy of sample B and C (QEMSCAN) represented in terms of weathering rates

3.2.3 Fe-sulfide liberation, association and grain size distribution

In addition to the sample mineralogy, on the micro scale, the liberation, association and grain size distribution of the Fe-sulfide minerals were considered, as characterisation tests are designed to have the minerals of interest (Mol) maximally liberated. The GSD of the minerals of interest is linked to the liberation behaviour of the material, which, in turn, has direct implications for the Mol exposed/available reactive surface area. The association of the unliberated Mols has implications for their subsequent reactivity when the associated minerals are (or are not) reacted away.

The Fe-sulfide liberation and association data are presented in Figure 3-4. Table 3-2 summarises the corresponding amount of liberated and unliberated Fe-sulfides in the samples alongside the number of Fe-sulfide-bearing particles assessed. Sample B was found to have 94% of the Fe-sulfide minerals liberated, while the Fe-sulfides in sample C were less liberated (71%). This difference in liberation was attributed to the difference in the grain size distributions (GSD) of the two samples (Figure 3-5). Sample C was found to have the finer Fe-sulfide GSD of the two samples, (I_{50} of 23 μ m and 15 μ m for samples B and C, respectively, and I_{90} of 55 μ m and 50 μ m for samples B and C, respectively). The importance of the Fe-sulfide liberation data is that it can potentially be used to apply a liberation correction to the calculated MPA providing a more likely estimate of the ARD characteristics, which has been proposed by Brough et al. (2018) and Elghali et al. (2018).

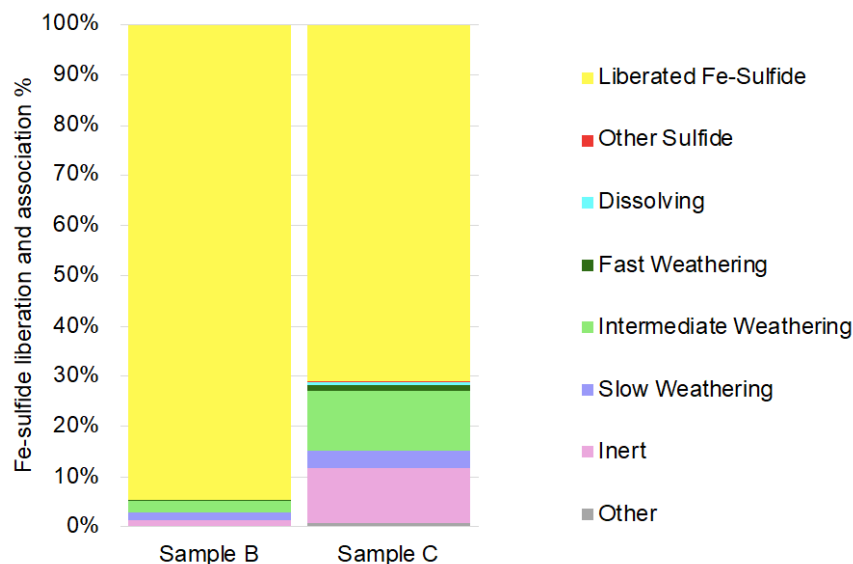
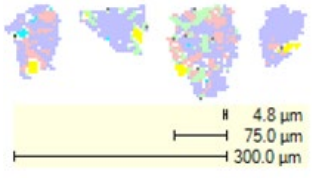

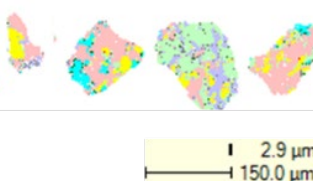
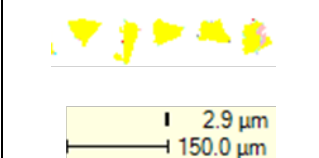


Figure 3-4 Fe-sulfide liberation and association for samples B and C (QEMSCAN). The association describes the interrelationship of unliberated Fe-sulfide mineral grains with other minerals present in the waste rock sample. These data correspond to those presented in Table 3-2

Table 3-2 The mass % distribution of the total Fe-Sulfide in the sample between liberated (>90% area exposed) and unliberated (<90% area exposed) categories. n = number of Fe-sulfide-bearing particles analysed. Selected false colour QEMSCAN particle images are included for visualisation (see Fig 3-4 for colour legend)

Fe-Sulfide Distribution	Unliberated		Liberated	
	Mass % Fe-Sulfide	Particles	Mass % Fe-Sulfide	Particles
Sample B (n=6395)	6%		94%	
Sample C (n=56068)	29%		71%	

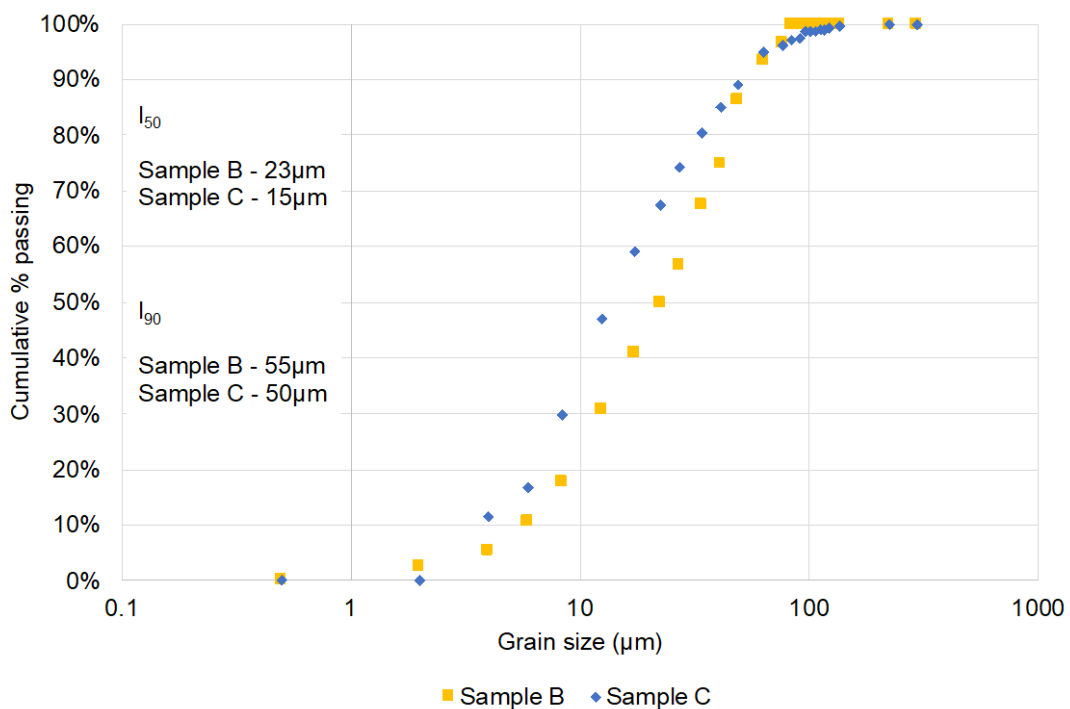


Figure 3-5 Fe-sulfide grain size distribution (GSD) for samples B and C (QEMSCAN). The I_{50} describes the size at which 50% of the Fe-sulfide grains are smaller than this size, while the I_{90} describes the size at which 90% of the Fe-sulfide grains are smaller than this size

3.3 Characterisation tests

3.3.1 Geochemical static tests

Acid rock drainage (ARD) characterisation generally includes a series of geochemical static tests, which can quickly provide a worst-case scenario estimation of the ARD formation potential through the use of

chemically aggressive test conditions. These tests are generally performed on fine samples ($-75\mu\text{m}$), to allow for maximal liberation of ARD-significant minerals, which maximises their reactivity. Acid-base accounting (ABA) tests are used as part of the screening process for the ARD potential of mine wastes and are used to determine the acid generating potential (AP) (also maximum potential acidity, MPA) and acid neutralising potential (NP) (also acid neutralisation capacity, ANC). The net acid producing potential (NAPP) is determined from the difference between ANC and MPA, with the MPA demonstrated by equation (13) and the NAPP by equation (14).

$$MPA = \%S \times 30.6 \quad (13)$$

$$NAPP = MPA - ANC \quad (14)$$

An additional test performed on samples is the net acid generation test (NAG), which is used to give an indication of whether the sample may be classified as potentially acid forming (PAF) (Smart et al., 2002; Weber et al., 2004), and may be plotted against the NAPP to provide a graphical representation of whether the sample is PAF, NAF or uncertain (UC) in terms of its acid formation potential (Smart et al., 2002). The NAG test is performed by reacting 2.5g of finely milled material with 15% hydrogen peroxide to enable rapid sulfide oxidation and facilitate simultaneous acid forming and neutralising reactions. Three variants of the NAG test have been developed, namely the single addition, sequential and kinetic NAG tests, which are used to account for geochemical variation between samples (Smart et al., 2002).

Although ANC and NAG tests are useful for placing a sample on the PAF/NAF/uncertain spectrum, they provide no information regarding the kinetics of the respective acid forming and neutralising reactions and neglect the effects of microbial catalysis at mine waste sites (Hesketh et al., 2010; Opitz et al., 2016a; Smart et al., 2002). Additional limitations of these tests include the assumption that all sulfur in the sample is pyritic, which yields an over- or underestimate of the AP if other sulfur-bearing species are present; the over-estimation of ANC caused by siderite or other Fe-carbonate minerals if not appropriately accounted for; and the inability of these tests to provide an indication of the lag times associated with ARD formation (Stewart et al., 2006; White et al., 1997). Errors may also arise in the interpretation of NP measurements due to neutralisation offered by non-carbonate minerals, as well as due to the uncertainty surrounding how these minerals would contribute to acid neutralisation in the field (Paktunc, 1999).

3.3.1.1 Experimental method

Static tests samples B and C were performed as described in Opitz et al. (2016a). ANC test was performed as outlined by the method in Weber et al. (2004) while the NAG test was performed as per methods outlined in Miller et al. (1997).



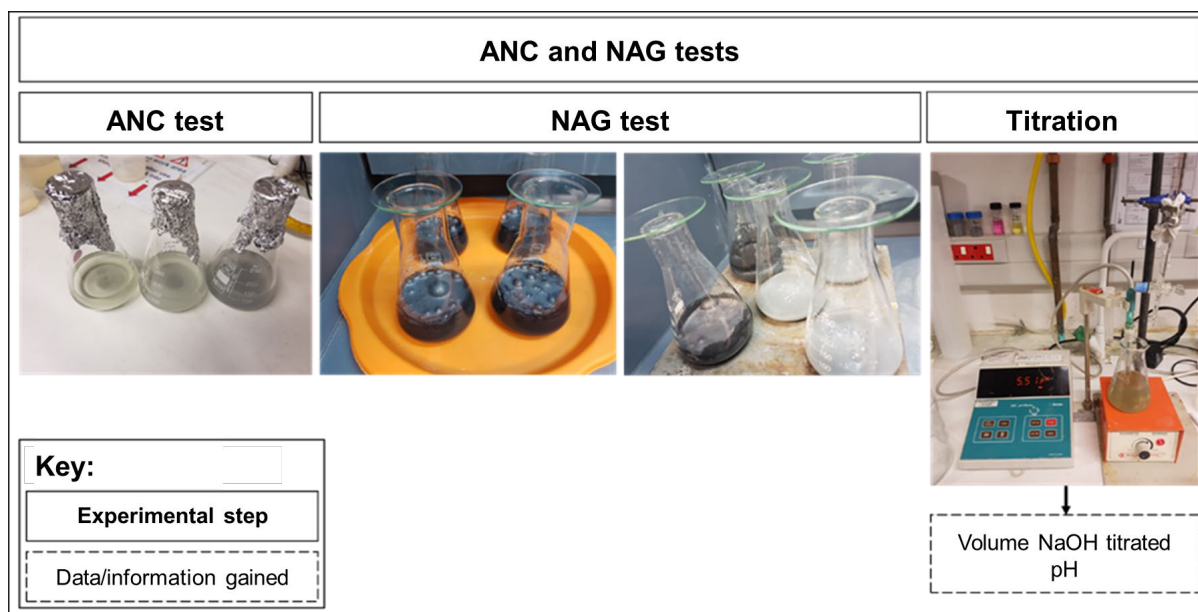


Figure 3-6 Images from left to right illustrate the ANC test after heating of the solutions, the NAG test prior to 24 hours of reaction with peroxide, NAG test during boiling step, titration set-up for both ANC and NAG tests

3.3.1.2 Sample characterisation

Sample B was found to be potentially acid forming (PAF), while sample C was characterised as uncertain (Figure 3-7). The MPA, ANC and consequently, the NAPP values were quite different for the two samples, with the values for sample C being considerably larger than those of sample B ($97.9 \pm 1.4 \text{ kg H}_2\text{SO}_4/\text{t}$ vs. $290 \pm 3.14 \text{ kg H}_2\text{SO}_4/\text{t}$, $91.9 \pm 0.01 \text{ kg H}_2\text{SO}_4/\text{t}$ vs. $187 \pm 0.06 \text{ kg H}_2\text{SO}_4/\text{t}$, and $6.0 \pm 1.4 \text{ kg H}_2\text{SO}_4/\text{t}$ vs. $102 \pm 3.1 \text{ kg H}_2\text{SO}_4/\text{t}$ for the MPA, ANC and NAPP values of samples B and C, respectively). These differences were arose primarily from the difference in mineralogy between the two samples. Table 3-1 and Figure 3-3 showed that sample C contained significantly more Fe-sulfide and dissolving minerals (31% and 13% Fe-sulfide and dissolving minerals, respectively) than sample B (8.6% and 2.2% Fe-sulfide and dissolving minerals, respectively), which accounted for the large MPA and ANC values. This suggests that the mineralogy of a sample plays a considerable role in the characterisation of a sample as PAF/NAF/UC.

The complete set of geochemical static test results is summarised in Table 3-3 and is graphically represented in Figure 3-7.

Table 3-3 Results of acid rock drainage characterisation tests for samples B and C. MPA = maximum potential acidity; ANC = acid neutralising capacity; NAPP = net acid producing potential; NAG = net acid generation; PAF = potentially acid forming; UC = uncertain

Sample	LECO (UCT) Total S %	MPA [kg H ₂ SO ₄ /t]	ANC [kg H ₂ SO ₄ /t]	NAPP [kg H ₂ SO ₄ /t]	NAG pH	ARD Classification
B	3.20 ± 0.05	97.9 ± 1.4	91.9 ± 0.01	6.01 ± 1.40	2.41 ± 0.01	PAF
C	9.47 ± 0.10	290 ± 3.1	187 ± 0.06	102 ± 3.1	6.45 ± 0.06	UC

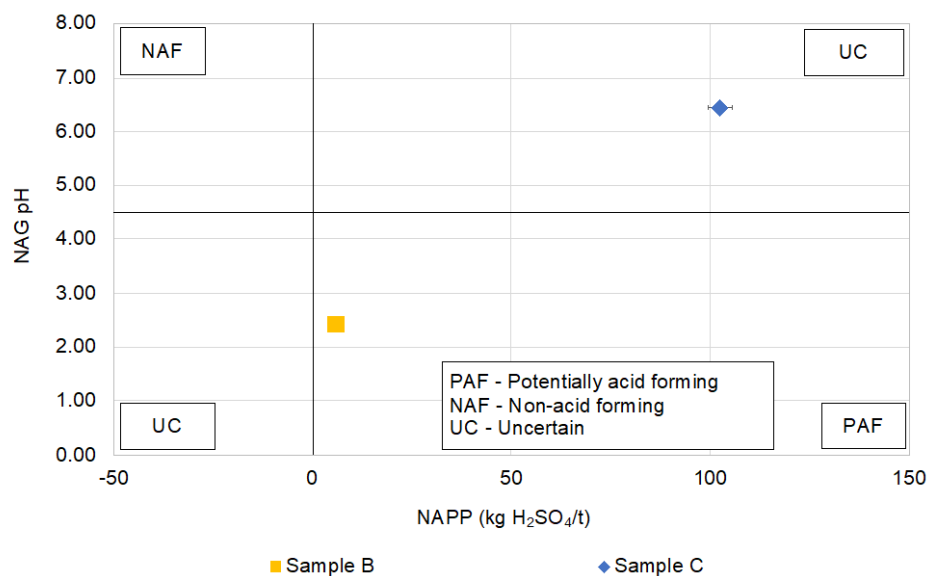


Figure 3-7 Graphical representation of acid rock drainage potentials for samples B and C (classification plot after Stewart et al. (2006))

3.3.2 UCT biokinetic test

The reaction kinetics in ARD processes are also integrally linked to the microbial activity at mine sites. Iron sulfide oxidation is catalysed by microbes in an acidic environment, with microbes catalysing the ferrous to ferric iron oxidation reaction that leaches exposed metal sulfide surfaces. ARD generation is also accelerated through the oxidation of sulfur-bearing intermediates resulting from sulfide oxidation (Hesketh et al., 2010; Vera et al., 2013). The microbially catalysed oxidation of pyrite is shown schematically in Figure 3-8.

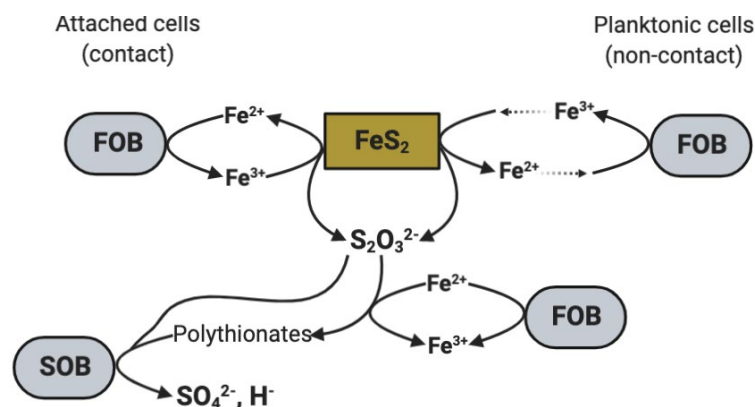


Figure 3-8 Diagrammatic representation of the oxidation of pyrite by iron-oxidising (FOB) and sulfur-oxidising (SOB) bacteria (adapted from Bryan, 2006)

Microbial activity in the UCT biokinetic test has been inferred to occur at redox potentials above 600mV and pH values below 5 (Bruynesteyn & Hackl, 1982; Hesketh et al., 2010). The latter condition may be correlated with the pH ranges provided for the mesophilic microbial species. Table 3-4 illustrates some of the microbial species present in waste rock dumps and includes the species used in the UCT biokinetic test. A more detailed list of microbial species present at mine waste sites may be found in Hallberg (2010).

Table 3-4 Optimal conditions for select mesothermal bacterial species present in waste rock dumps and those used in the UCT biokinetic test developed by Hesketh et al. (2010) (Schippers et al., 2014)

Bacterial species	Optimum pH	pH range	Optimum temperature	Temperature range
<i>At. ferrooxidans</i>	2.5	1.3-4.5	30-35°C	10-37°C
<i>At. thiooxidans</i>	2.0-3.0	0.5-5.5	28-30°C	10-37°C
<i>L. ferrooxidans</i>	1.5-3.0	1.3-4.0	28-30°C	-
<i>L. ferriphilum</i>	1.3-1.8	-	30-37°C	Up to 45°C
<i>At. caldus</i>	2.0-2.5	1.0-3.5	45°C	32-52°C
<i>S. benefaciens</i>	1.5	>0.8	38.5°C	<47°C

The University of Cape Town (UCT) biokinetic test was developed to address the shortcomings of existing characterisation and prediction tests by accounting for microbial effects and running for a shorter time frame (90 days) than the humidity cell test (Hesketh et al., 2010). The measured variables include but are not limited to the pH and the redox potential (Hesketh et al., 2010). This test, as stated by Hesketh et al. (2010) aims to “provide information on the potential and likelihood of acidification upon microbial colonisation as well as the relative kinetics of the acid-consuming and acid-producing reactions”. The effectiveness of this test has been proven for various waste types, both for hard rock species and coal, as shown by Broadhurst et al. (2013), with the results of this test being meaningful from the perspective of long-term ARD generation at size fractions below 315µm. The UCT batch biokinetic test was also found to enhance and complement the results obtained from conventional geochemical static tests (Broadhurst et al., 2013; Dyantyi et al., 2013; Opitz et al., 2016a).

3.3.2.1 Experimental method

The method for the UCT batch biokinetic test was performed as outlined by Opitz et al. (2016a) building on the method described by Hesketh et al. (2010). The test was performed for sample C during the course of the current study, while the results for sample B were obtained from Opitz et al. (2016a). The tests required a sample mass of 7.5g, with the rotary sample divider being used to split the sub-samples representatively to allow for three replicates per test. Inoculated non-pH-controlled experiments were reported for sample B and performed for sample C. A pH-controlled experiment (with pH controlled to pH 2) was performed for sample C to assess microbial activity following the depletion of the neutralising capacity.

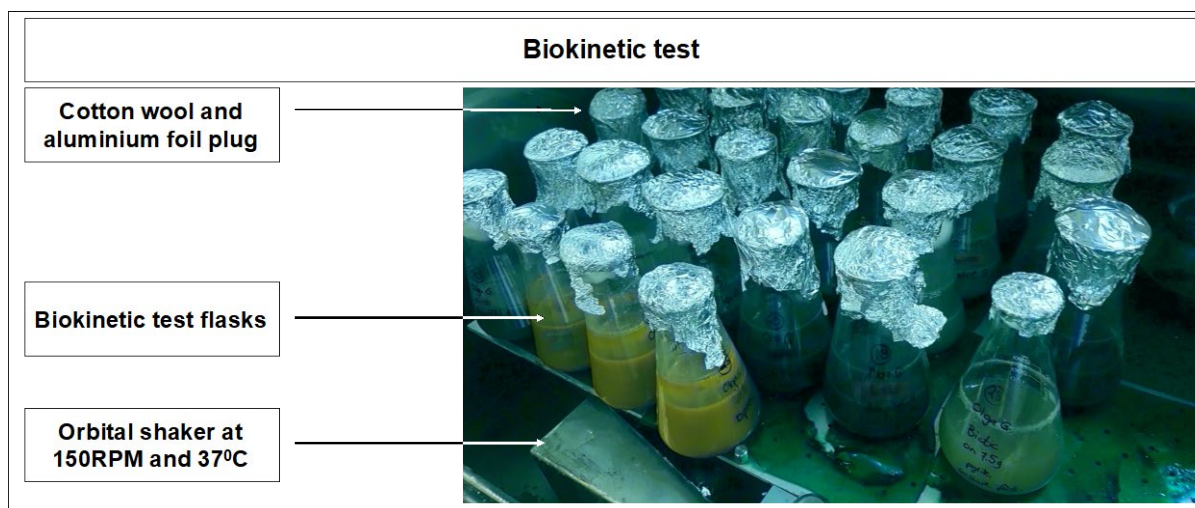


Figure 3-9 UCT batch biokinetic test experimental set-up

3.3.2.2 Sample characterisation

The pH profiles for the UCT batch biokinetic tests are presented in Figure 3-10 for samples B and C. The non-pH-controlled pH profile for sample B became circumneutral within the first few days of the test, rising up to just below 8. This was attributed to the presence of carbonate minerals (2.2%) in the sample (Opitz et al., 2016a). The pH gradually decreased over the duration of the test but remained above pH 6. Similar behaviour was observed for the non-pH-controlled sample C, where the high carbonate content (13%) pushed the pH up to 8 (higher than for sample B). Additionally, sample C maintained a pH above 7 over the duration of the test. These high pH conditions were unfavourable for high microbial activity (see Table 3-4, (Schipper et al., 2014)), irrespective of the high Fe-sulfide content of the two samples (8.6% and 31% for samples B and C, respectively).

The pH-controlled experiment for sample C was used to provide an indication of microbial behaviour in the test flasks once neutralisation capacity was depleted. In these tests, the pH profile decreased over the first 10 days with pH control, dropping spontaneously (without pH control requirement) to pH 1.4 after day 10. This drop in pH to below was attributed to the dissolution of abundantly present pyrrhotite. The pH then rose steadily to 1.9 by day 21, which was thought to occur, in part, due to the dissolution of intermediate weathering minerals (7.6% Fe-mica, 4.7% chlorite) (Becker et al., 2015).

The redox potential plot (Figure 3-11) was used alongside the pH profile to infer microbial activity. Higher redox potentials indicate higher relative concentrations of ferric iron as opposed to ferrous iron, from which microbial activity is inferred. For the non-pH-controlled profiles of both samples, the absence of microbial activity due to circumneutral pH was supported by the redox potential profile remaining well below the 650mV line. For the pH-controlled experiments, the redox potential began increasing after day 5, with a prominent increase seen after day 21, increasing to around 720mV by day 29.

These profiles suggest that although in a batch environment the presence of neutralisation potential in the form of dissolving minerals impedes microbial activity, once these dissolving minerals are depleted (as in the pH-controlled tests), microbial activity increases. This was supported by the low pH for the duration of the test after pH control was stopped and the rise and maintenance of the high redox potential.

Although the mineralogy was found to be different for samples B and C, the presence of dissolving minerals even as low as 2.2% (sample B) was considered sufficient to raise the pH up to conditions unfavourable for microbes, as seen for non-pH-controlled sample B. The pH profile did, however, drop over the duration of the test, which was attributed to the partial depletion of the available dissolving minerals. This drop was not as prominent for the non-pH-controlled experiment for sample C, which

had a larger dissolving mineral content (13%). What is important, however, is that once the neutralisation capacity was depleted by pH-control to pH 2 (pH-controlled sample C), the microbes became active, increasing the redox potential to 600mV by day 25 and maintaining the low pH until day 90. Additionally, the presence of intermediate weathering minerals such as Fe-mica and chlorite were thought to contribute to the slight rise in pH of the pH-controlled profile following the pH drop to 1.4.

It is important to note that the large error bars on some data points are present due to variation between the replicate flasks, as it is suspected that the microbes adapted differently to their environment in each replicate flask. Although all flasks had similar growth curves, these growth curves might have had similar gradients on different sampling days due to possible variation in initial inoculum cell number.

Similarities in the non-pH-controlled profiles between samples B and C may be explained by the similar lack of microbe behaviour when pH conditions were unfavourable for microbial activity due to the pH conditions introduced by presence of calcite, as indicated by the bulk mineralogy.

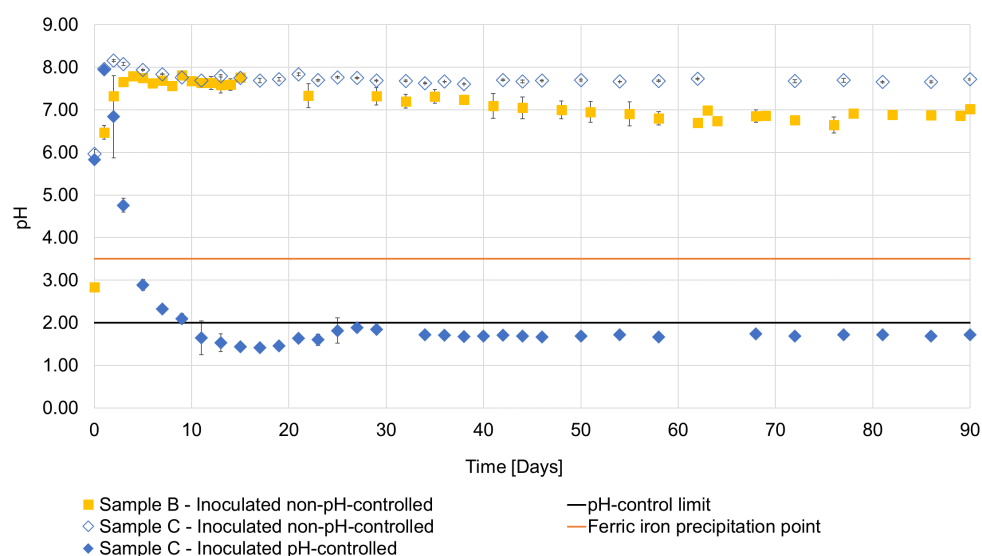


Figure 3-10 UCT batch biokinetic test pH profile. pH-control limit line represents the pH to which the experimental flasks were adjusted each day, with the rise in pH attributed to the presence of neutralising minerals. The error reported is that obtained from 1x the standard deviation, which indicates the variation between the triplicate samples used in the test

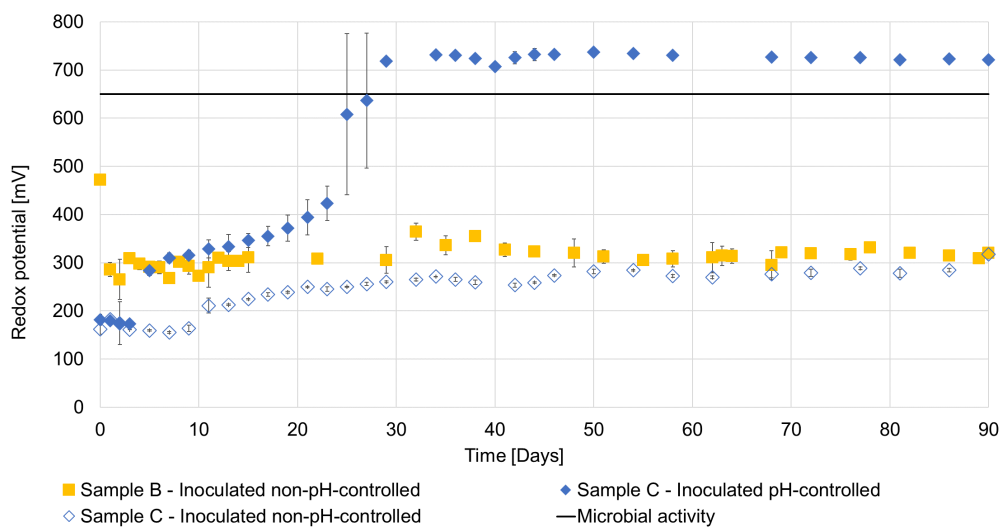


Figure 3-11 UCT batch biokinetic test redox profile. The error reported is that obtained from 1x the standard deviation, which indicates the variation between the triplicate samples used in the test

4 ARD characterisation and prediction on the meso scale

Overview: This chapter focuses on addressing objective number two that seeks to quantify the effect of mineral texture on ARD characterisation at the meso scale ($>1\text{mm}$), specifically in the context of laboratory kinetic tests.

4.1 Samples and sample preparation

The samples selected for meso scale analyses were prepared similarly to the procedure outlined in section 3.1 with the adjustments below.

Sub-samples were screened to pass through a $6700\mu\text{m}$ screen. 1kg sub-samples of this material were selected for kinetic testing and mineralogical and textural analyses. The latter sub-samples were dry screened into discrete size fractions of $-6700/+2000\mu\text{m}$, $-2000/+1000\mu\text{m}$, $-1000/+425\mu\text{m}$, $-425/-150\mu\text{m}$ and $-150/0\mu\text{m}$.

The bulk particle size distribution for samples B and C is provided in Figure 4-1.

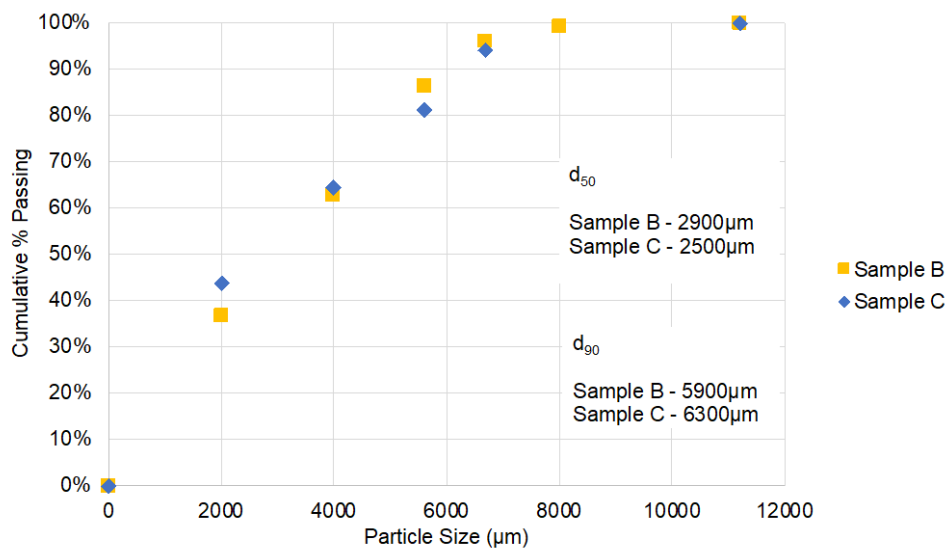


Figure 4-1 Particle size distribution for the HCT feed material of samples B and C

The d_{50} of samples B and C were found to be $2900\mu\text{m}$ and $2500\mu\text{m}$, respectively, while the d_{90} of these samples were $5900\mu\text{m}$ and $6300\mu\text{m}$, respectively. This difference in particle size distributions was thought to arise due to sample B being received as a crushed waste rock sub-sample, whereas sample C was received as a drill core sub-sample. Additionally, the difference in mineralogy and texture between samples B and C would affect the breakage of the material, and therefore the PSD.

The top size of $6700\mu\text{m}$ was chosen for the HCT feed material as it was the closest available screen size to that prescribed for humidity cell testing ($6300\mu\text{m}$, ASTM, 2013). Overall, most of the mass (over 50%) for both samples was obtained in the $-6700/+2000\mu\text{m}$ size fraction.

4.2 Mineralogy and texture

The assessment of meso scale texture of humidity cell test feed material has been gaining popularity in the past few years (Brough et al., 2017, 2018; Elghali et al., 2018, 2019), with important textural parameters for this scale being identified as the degree of liberation of the Mols (acid forming and neutralising minerals), their grain size distribution, mineral associations, reactivity and the available reactive surface areas of acid forming and neutralising minerals (Parbhakar-Fox et al., 2011; Brough et al., 2017, 2018; Elghali et al., 2018, 2019).

A waste rock dump/heap may consist of rocks ranging from very fine, powdered material to enormous boulders, therefore particle size (and the particle size distribution) is an essential parameter to consider when discussing ARD characterisation, prediction and generation (Elghali et al., 2018, 2019). The particle size distribution for coarser material needs to be considered alongside the grain size distribution, as the larger the particle size in relation to the mineral grain size, the higher the possibility of encapsulation (rather than liberation) of the Mol. In the context of humidity cell test work the relationship between the Fe-sulfide GSD and liberation, and the effect of these parameters on the rate of acidic leachate generation was shown by Brough et al. (2017).

On the meso scale there is an increased likelihood of ARD-significant mineral encapsulation in coarser size fractions. This, alongside the potentially long-time frames for acidic leachate formation, underlines the importance of assessing the liberation, association, GSD and the distribution of these minerals throughout the HCT feed material on a size-by-size basis to enable improved interpretation of prediction test results and the potential of waste material to generate ARD.

When undertaking mineralogical and textural analyses a common area of concern is the statistical soundness of the measurements, especially for larger particle sizes. Statistical soundness generally decreases with a decrease in the number of particles analysed, while the number of particles analysed, in turn, tends to decrease as the particle size increases due to the plausible number of particles per sample block and the associated costs of measurement. It is therefore essential to ensure a sufficient number of Mol-bearing particles is assessed to ensure data validity. Additionally, laboratory analyses assess sub-samples that are many orders of magnitude smaller than the parent material. This introduces the question of how representative these small sub-samples actually are of the parent material (Petersen et al., 2004). Sampling errors often far exceed those arising from analyses (Carrasco et al., 2004; Petersen et al., 2005). Consequently, experiments performed on the sub-sampled material may yield data which are difficult to correlate across various tests and/or relate to the behaviour of the parent sample. Quantitative textural analysis, however, does provide a means of quantifying sampling errors with tools such as 'Gy's equation' (equation (15)), which relies on the mineralogical and textural properties of the material to estimate the sampling errors involved. During this study, sampling errors for the largest material at the masses used for the tests (both chemical and textural) were found to be under 10%, which may be considered as realistically acceptable (François-Bongarçon and Gy, 2002).

$$\sigma_r^2 = \sum_{i=1}^N \left(\frac{1}{M_s} - \frac{1}{M_L} \right) f c g l d_i^3 \quad (15)$$

Variables used: σ_r = FSE variance; M_s = sub-sample mass (g); M_L = mass of the parent sample (g); f = shape factor (generally approximated as 0.5); g = granulometric/grain size distribution factor; c = mineralogical composition factor (sometimes also referred to as the "constitution" factor); l = liberation factor; d_i = d_{95} of the sample (cm)

An additional source of error in 2D measurements is the stereological bias. It should be noted that although the stereological bias was acknowledged in this study, it was not quantitatively accounted for. It was assumed that the complexity of the texture, as well as the fine-grained nature of the majority of the Mols decreased the magnitude of the stereological bias (Spencer & Sutherland, 2000). Additionally, although the correction for stereological bias is often recommended, some researchers have argued that potentially for a majority of ore textures the application of correction factors to 2D mineralogical and



textural data could actually decrease the accuracy of the data rather than enhance it (Lätti & Adair, 2001). For the purposes of this study the stereological bias was not explicitly corrected for, even though this is a recommended mathematical exercise that has been investigated in much detail in recent years (Ueda et al., 2016, 2017, 2018).

4.2.1 Experimental method

The textural and mineralogical assessments were performed as described in section 3.2.1 with the following adjustments.

The size fractions used for QEMSCAN analyses were -6700/+2000 μ m, -2000/+1000 μ m, -1000/+425 μ m, -425/+150 μ m, and -150/+0 μ m. Size fractions larger than 1000 μ m were prepared as 70x70mm blocks (see Figure 4-2), while size fractions smaller than 1000 μ m were prepared as QEMSCAN block vertical sections (see Figure 3-2). This was done to enable a larger number of particles to be analysed during textural and mineralogical analyses, thereby attempting to decrease the analytical and sampling errors. When making the 70x70mm sample blocks, the particles were allowed to settle to the bottom of the block in the epoxy-resin mixture. Thereafter the sample blocks were ground down to reveal the particle cross-sections and hand-polished (as opposed to the machine polishing of standard-sized blocks). Vertical sections were used to decrease the settling effects caused by difference in the mass of the individual particles. This approach was expected to improve the sample representativeness and data reliability (Pooler & Dold, 2017).

When analysing the meso scale sample blocks, each discrete size fraction had measurement settings adjusted for the particle size. These are provided in Table 4-1.

Table 4-1 Measurement settings used during QEMSCAN operation for meso scale size fractions. FI = field image; PMA = particle mineralogical analysis

Measurement parameter	-6700/+2000	-2000/+1000	-1000/+425	-425/+150	-150/+0
Point spacing	15 μ m	15 μ m	10 μ m	5 μ m	3 μ m
Field size	2500	2500	1500	1500	1500
Measurement type	FI, PMA (include boundary)	FI, PMA (include boundary)	FI, PMA (include boundary)	FI, PMA (exclude boundary)	PMA (exclude boundary)

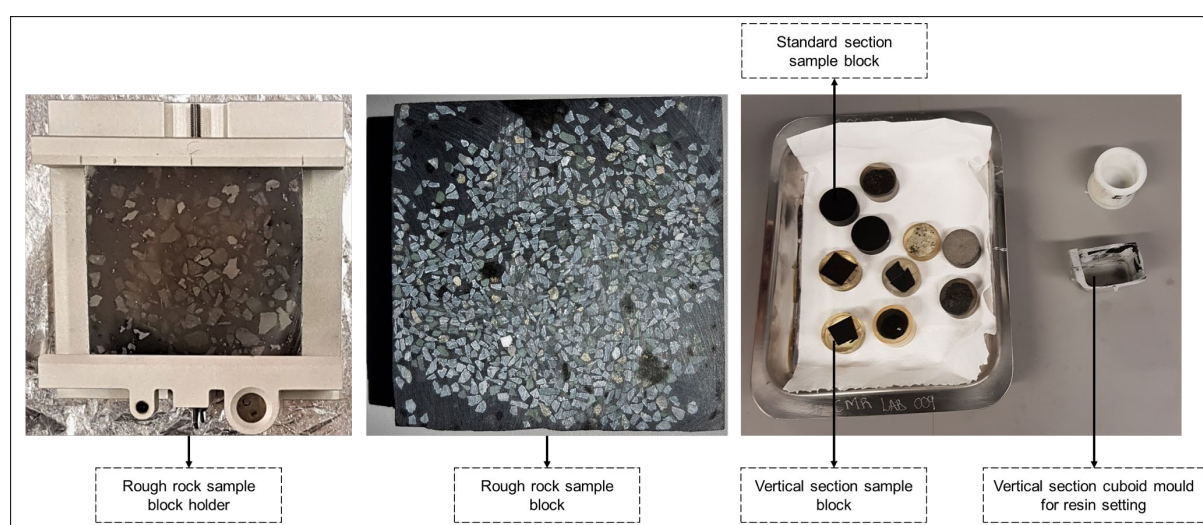


Figure 4-2 Images from left to right: 70x70mm rough rock sample block holder with sample block; 70x70mm rough rock sample block; standard and vertical section sample blocks (30mm diameter)

4.2.2 Bulk mineralogy

The sized HCT feed mineralogy data by reactivity grouping for samples B and C are presented in Figure 4-3, with these data being supported by Table A-3 and Table A-4 in the Supplementary Content section. From Figure 4-3 the mineralogical distribution follows the bulk mineralogy given in Figure 3-3. Sample B mineralogy was dominated by inert (quartz), slow weathering (K-feldspar, plagioclase-feldspar, magnetite) and intermediate weathering (Fe-mica, chlorite) minerals. Sample C mineralogy was dominated by inert minerals (quartz, titanite) and Fe-sulfides (pyrrhotite), followed by the dissolving (calcite), intermediate weathering (chlorite, Fe-mica) and slow weathering (K-feldspar) groups. This distribution of the minerals was found to be relatively well-maintained across the size fractions, with some deviation occurring across the groupings. This was more evident for the -150/+0 μ m size fraction, which showed a preferential deportment of Fe-sulfides into the finer fractions, particularly for sample C, which had the larger Fe-sulfide content. This suggested preferential breakage or more brittle behaviour of the softer Fe-sulfide minerals (Evans, 2010). The size-by-size mineralogy for samples B and C is provided in the Supplementary Content section, Table A-3 (sample B) and Table A-4 (sample C).

The majority of the sample mass (>50%) was concentrated in the -6700/+2000 μ m size fraction based on the PSD (Figure 4-1). This suggested that this size fraction would be the most important to consider for the purposes of HCT behaviour and for textural analyses. This is illustrated in Figure 4-4.

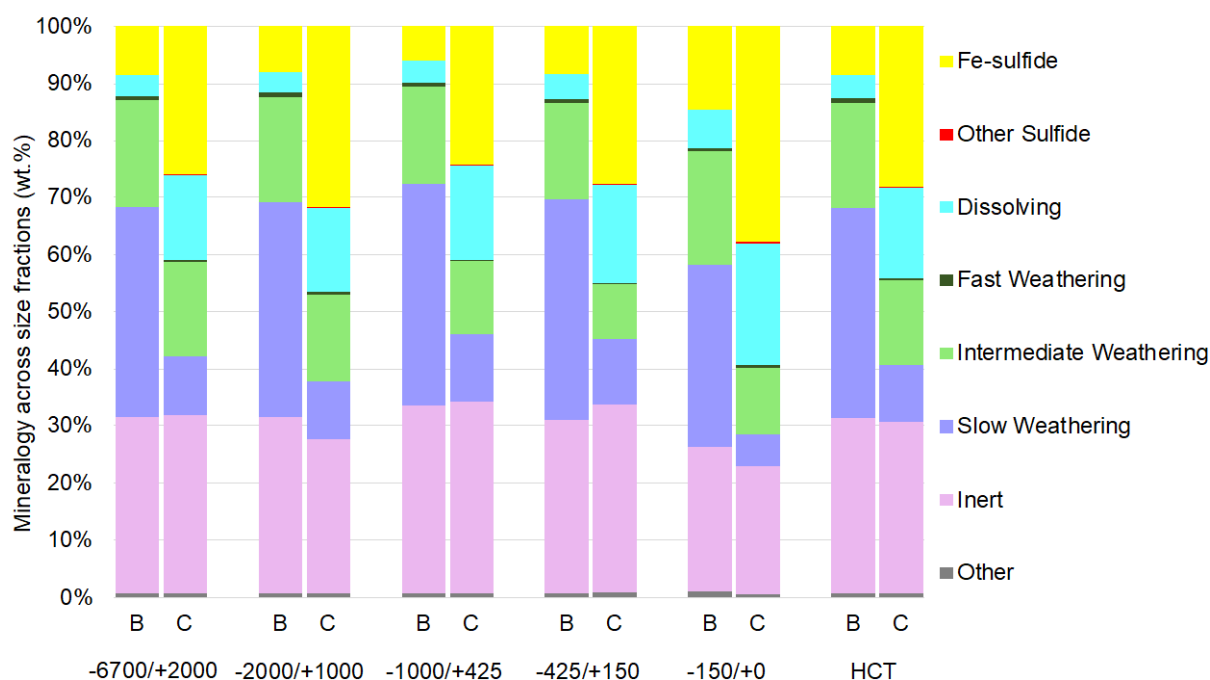


Figure 4-3 Mineralogy by particle size fraction as well as the reconstituted bulk mineralogy of the HCT feed for samples B and C

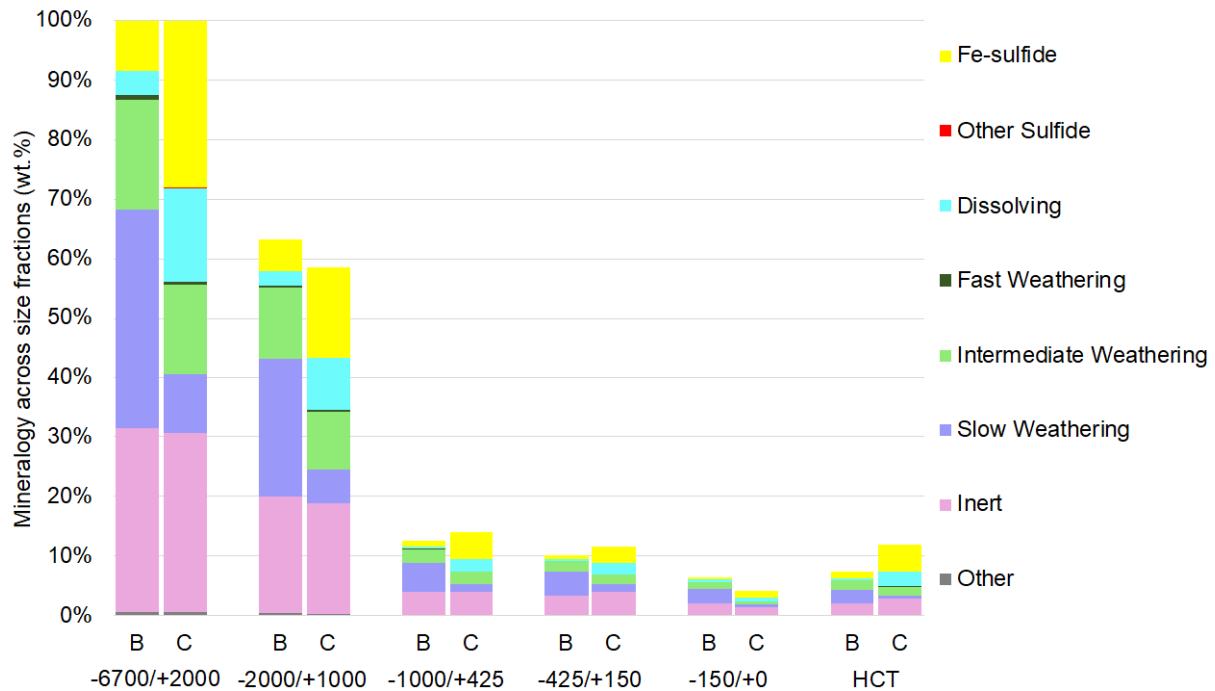


Figure 4-4 Mineralogy by particle size fraction as well as the reconstituted bulk mineralogy of the HCT feed for samples B and C, with a 100% indicating the full sample mass

4.2.3 Fe-sulfide liberation, association and grain size distribution

The liberation and association of the Fe-sulfide material in samples B and C was represented in terms of the relative weathering rates of mineral groups, as in section 3.2. These results are presented in Figure 4-5, which corresponds with Table 4-2.

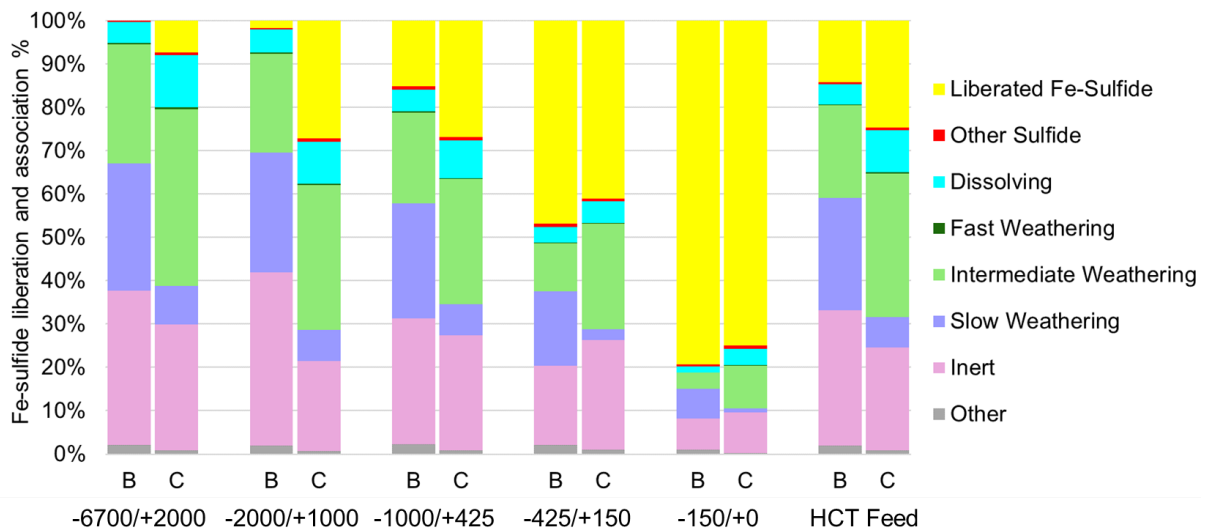


Figure 4-5 Fe-sulfide liberation and association for samples B and C (QEMSCAN). The association describes the interrelationship of unliberated Fe-sulfide mineral grains with other minerals present in the waste rock sample. These data correspond to those presented in Table 4-2

Sample B contained Fe-sulfide minerals in the -6700/+2000 μ m size fraction that were entirely associated with other minerals (meaning that all the Fe-sulfide material in this size fraction had less than 90% of its area exposed to the environment/atmosphere). As the size fraction decreased, the fraction of liberated Fe-sulfide material increased, while the amount of locked Fe-sulfides decreased. Overall, the liberation was greater for sample C than for sample B.

The Fe-sulfide association distribution for size fractions in sample B maintained their association predominantly to intermediate weathering minerals, followed by associations to inert and slow weathering minerals. The association to dissolving minerals decreased with decreasing size fraction, but this association has the potential to provide immediate acid neutralisation for acid formed from the dissolution of associated Fe-sulfide material.

For the reconstituted HCT feed, sample B was less liberated (14% liberated) than sample C (25% liberated). Although this was consistent with the larger size fractions (-6700/+2000 μ m, -2000/+1000 μ m and -1000/+425 μ m) where sample C showed a larger portion of liberated Fe-sulfides, at size fractions smaller than -1000/+425 μ m sample B exhibited greater Fe-sulfide liberation. The PSD of the material was important to consider in conjunction with the liberation data, as in this case at least 50% of the sample material was concentrated in the largest particle size fraction. For sample C, liberation was already present in this size fraction (7%) whereas sample B contained no liberated Fe-sulfides in this fraction. The larger overall liberation for sample C than for sample B therefore indicates that the larger size fractions control the textural characteristics of the HCT feed material.

Table 4-2 The mass % distribution of the total Fe-Sulfide in the sample between liberated (>90% area exposed) and unliberated (<90% area exposed) categories. n = number of Fe-sulfide-bearing particles analysed

Sample	Size fraction (μ m)	n	Unliberated	Liberated
			Mass % Fe-Sulfide	Mass % Fe-Sulfide
B	-6700/+2000	470	100%	0%
	-2000/+1000	1297	98%	2%
	-1000/+425	1120	85%	15%
	-425/+150	3060	53%	47%
	-150/+0	46326	21%	79%
	HCT Feed	52273	86%	14%
C	-6700/+2000	465	93%	7%
	-2000/+1000	1302	73%	27%
	-1000/+425	1316	73%	27%
	-425/+150	2215	59%	41%
	-150/+0	55599	25%	75%
	HCT Feed	60897	75%	25%

The liberation characteristics were also related to the Fe-sulfide grain size distribution. The grain size distribution (GSD) of minerals was important to consider, as the GSD has a direct effect on the liberation characteristics of minerals. This has been shown to be valid for ARD kinetic testing (Brough et al., 2017).



The bulk grain size distribution (GSD) for the Fe-sulfide minerals (predominantly pyrite for sample B and pyrrhotite for sample C) is provided in Figure 4-6. To differentiate the GSD from the PSD, the 50% and 90% size distribution points were labelled as I_{50} and I_{90} , respectively for the GSD as opposed to the d_{50} and d_{90} used to denote these points for the PSD.

Although the I_{50} of the GSD for samples B and C was similar (118 μ m and 105 μ m, respectively), the I_{90} showed that sample C (550 μ m) had an overall coarser Fe-sulfide GSD than sample B (210 μ m). These I_{50} and I_{90} values for samples B and C were considerably smaller than the PSD d_{50} and d_{90} for the samples (2900 μ m and 5900 μ m, and 2500 μ m and 6300 μ m for the d_{50} and d_{90} of samples B and C, respectively), which indicated potential for a higher degree of Fe-sulfide encapsulation, as seen in Figure 4-5. Additionally, the higher degree of encapsulation for sample C in the finer size fractions was supported by it having the comparatively finer Fe-sulfide grain size than sample B below the 51% cumulative passing point.

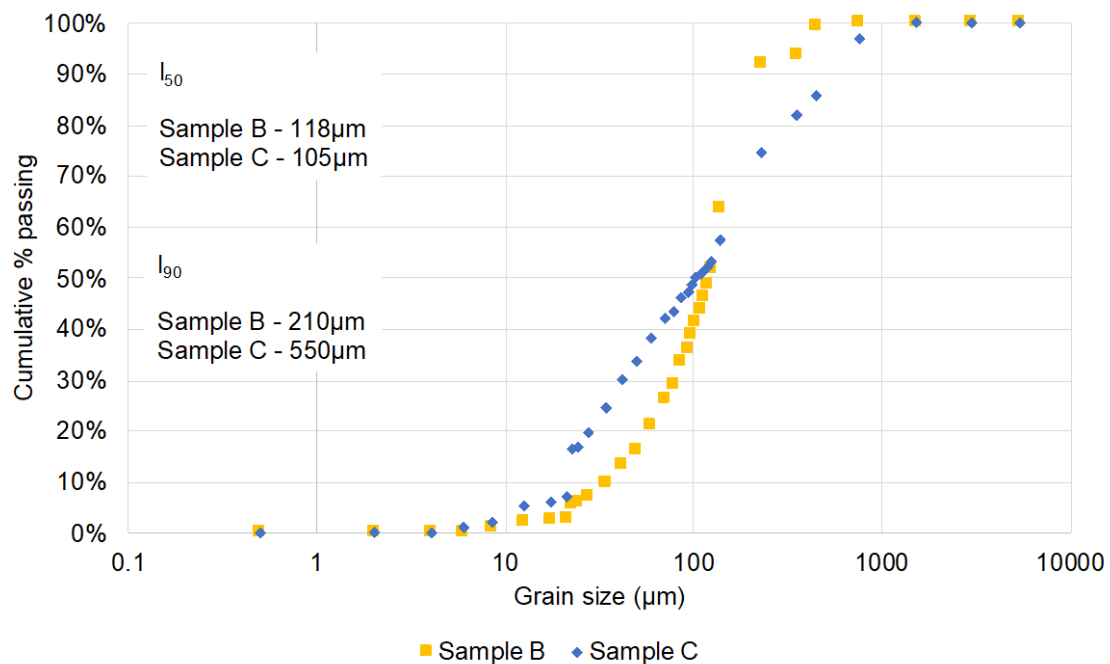


Figure 4-6 Unsized Fe-sulfide mineral grain size distribution for meso scale samples B (n=52273) and C (n=60897) where n is the total number of dissolving mineral-bearing particles analysed

Figure 4-7 provides select false-colour images of the Fe-sulfide-bearing particles in samples B and C. The images show that the Fe-sulfide material was found in a variety of textures, including disseminated, massive and veined Fe-sulfides. This variation in texture affects the propensity of the waste material to generate ARD (Parbhakar-Fox, 2012, Parameter C). It is important to note, that although this textural variation of Fe-sulfide minerals is evident when looking at individual particles, quantitative QEMSCAN reports (such as those providing GSD data) may be more difficult to interpret with consideration for this variation. In such cases, the value of simply observing particle textures to complement the quantitative GSD cannot be overemphasized.

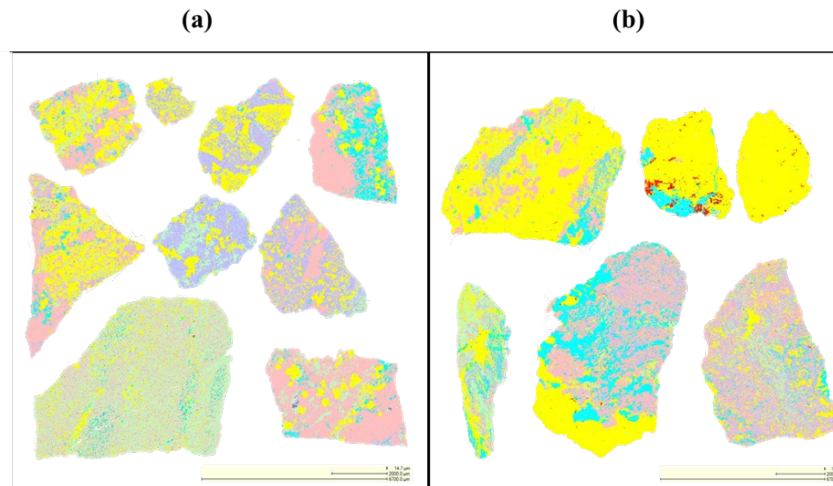


Figure 4-7 False-colour images of the Fe-sulfide-bearing particles in samples B (a) and C (b). See Figure 4-5 for colour legend

4.2.4 Dissolving mineral liberation, association and grain size distribution

In addition to the Fe-sulfide texture, the samples were assessed for dissolving mineral liberation, association and grain size distribution. These data are presented in Figure 4-8 and Figure 4-9. The trend in degree of liberation followed closely that of the Fe-sulfide material (limited liberation in particles larger than 1mm, followed by increasing liberation with decreasing particle size). Additionally, it should be noted that unliberated dissolving minerals appeared to be associated predominantly with inert, intermediate weathering and Fe-sulfide minerals. The latter point is important, as dissolving minerals associated with Fe-sulfide material may provide locally available neutralisation potential for acid formed from the oxidation of the associated Fe-sulfide minerals.

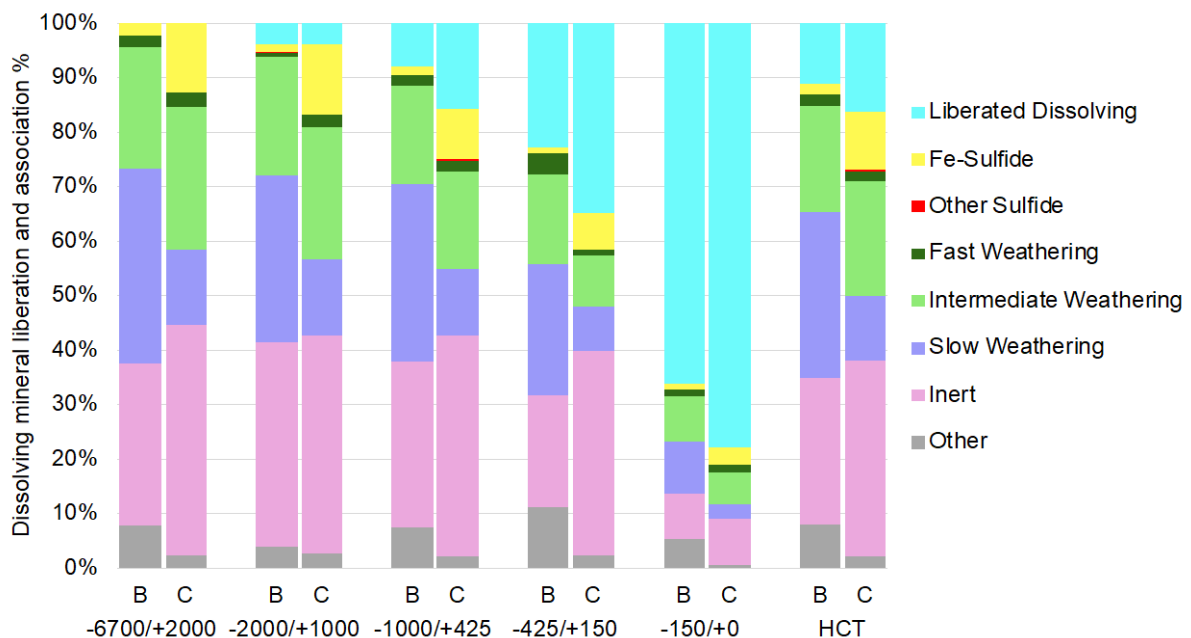


Figure 4-8 Dissolving mineral liberation and association for samples B (n=81804) and C (n=146442) (QEMSCAN), where n is the total number of dissolving mineral-bearing particles analysed. The association describes the interrelationship of unliberated dissolving mineral grains with other minerals present in the waste rock sample

The dissolving mineral GSD for samples B and C showed that sample C had a slightly coarser grain size than sample B at the I_{50} point (55μm vs. 65μm for samples B and C, respectively) and a slightly

finer dissolving mineral grain size than sample B at the I_{90} point (185 μm vs. 165 μm for samples B and C, respectively). This was consistent with the liberation of sample C becoming more than that of sample B only in the finer size fractions (<1000/ \pm 425 μm and finer), similarly to the liberation behaviour of the Fe-sulfide minerals.

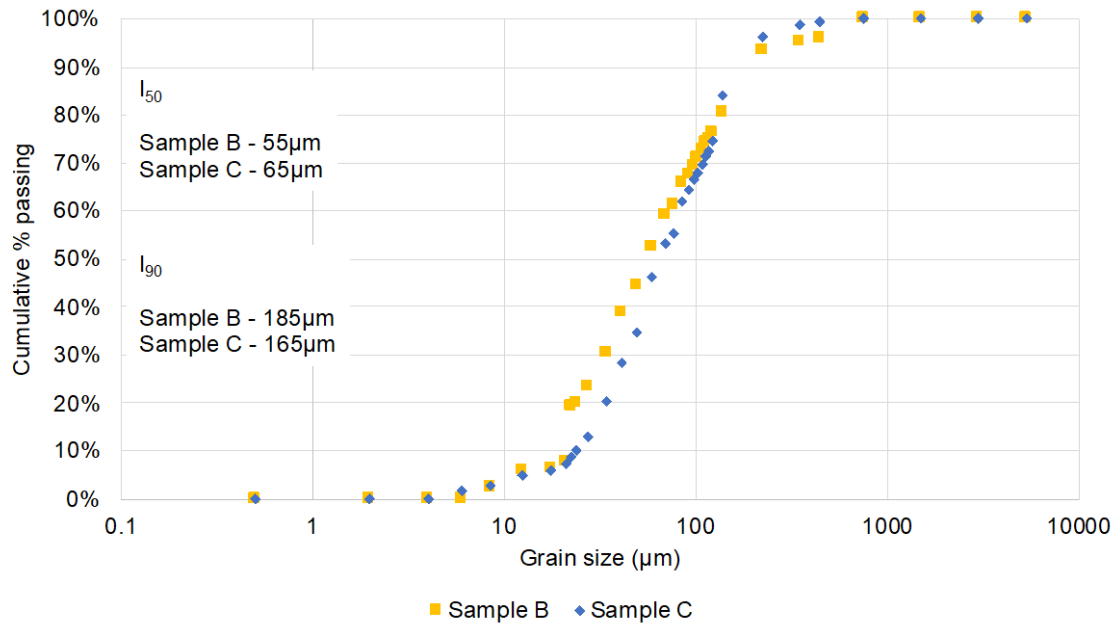


Figure 4-9 Unsized dissolving mineral grain size distribution for meso scale samples B ($n=81804$) and C ($n=75011$) where n is the total number of dissolving mineral-bearing particles analysed

4.3 Humidity cell tests

The humidity cell test (ASTM, 2013) is the more commonly used kinetic test for the prediction of the rates of ARD formation and is mostly performed on samples that have been characterised by geochemical static tests to be uncertain (UC) or potentially acid forming (PAF) and to obtain data pertaining to the lag time for acid formation (Parbhakar-Fox & Lottermoser, 2015). Additionally, data obtained from the HCT has also been applied to the formulation of geochemical models for ARD generation (Maest & Nordstrom, 2017).

The HCT ASTM (2013) procedure subjects a 1kg coarse ($d_{95} = 6.3\text{mm}$) sample to a dry/humid air cycle and a subsequent flush/leach with water (ASTM, 2013). Some main shortcomings of this method are the high associated cost (up to \$5000/20 weeks, 2015) and the long and poorly defined timescales (months to years) for the obtaining of meaningful data (ASTM, 2013; Brough et al., 2017; Parbhakar-Fox & Lottermoser, 2015). These time scales can range from a minimum of 20 weeks (Smart et al., 2002), up to 60 weeks or even years (INAP, 2009; Lengke et al., 2010; Brough et al., 2013, 2017). Additionally, the HCT procedure does not necessarily mimic natural climatic conditions present at mine sites, with considerable challenges being faced with upscaling of the results to the field scale (Parbhakar-Fox & Lottermoser, 2015).

More recently, humidity and column cell test work has been combined with textural assessment (see section 2.2) to assess the controls in column leachate generation and to gain an improved understanding of how results at the meso-scale interlink with those of standard static test methods (Brough et al., 2017, 2018; Elghali et al., 2019); however, textural and mineralogical assessments are not routine practices in the context of standard ARD test methodologies due to the assumption that mineralogical/textural changes would be limited over the minimum duration of these tests (Parbhakar-Fox et al., 2013).

4.3.1 Experimental method

The HCT results for sample B were obtained from (Opitz et al. unpublished). The samples were prepared as described in section 4.1, with the $\pm 3\text{kg}$ sub-sample being split into $\pm 1\text{kg}$ sub-samples using a rotary sample divider, as required by the ASTM (2013) experimental procedure.

The humidity cell test was performed following the procedure outlined in ASTM (2013) Option A for samples B and C. The samples were prepared for the test by passing $\pm 1\text{kg}$ of the coarse, milled sub-sample through a 6.3mm screen. The closest screen to this size available was 6.7mm, therefore this was used. Two replicates were run for each of the water-fed HCTs for samples B and C.

The volume of leach solution (de-ionised water) used for the flood leach was 1000mL for sample B and 500mL for sample C. Following the addition of the leach solution, the sample was left to remain in contact with the solution for two hours after which time the columns were drained and the leachate was collected. The mass of the flood leach solution was recorded before addition to each column and after collection of the leachate into collection bottles. Following the flood leach the columns were allowed to rest for 24h, after which a three-day dry air cycle was started, followed by a three-day humid air cycle. The air was supplied to the column at a flow rate of $\pm 5\text{L/min}$ and the humidity for the three-day humid air cycle was controlled using a hot plate at a constant temperature of approximately 30°C . The filtered leachate solution was assessed for pH, redox potential, total iron and sulfate ions. The iron assay was performed using the 1-10 phenanthroline method (Komadel & Stucki, 1988), while the sulfate was assayed using turbidimetric assessment (APHA, 1999).

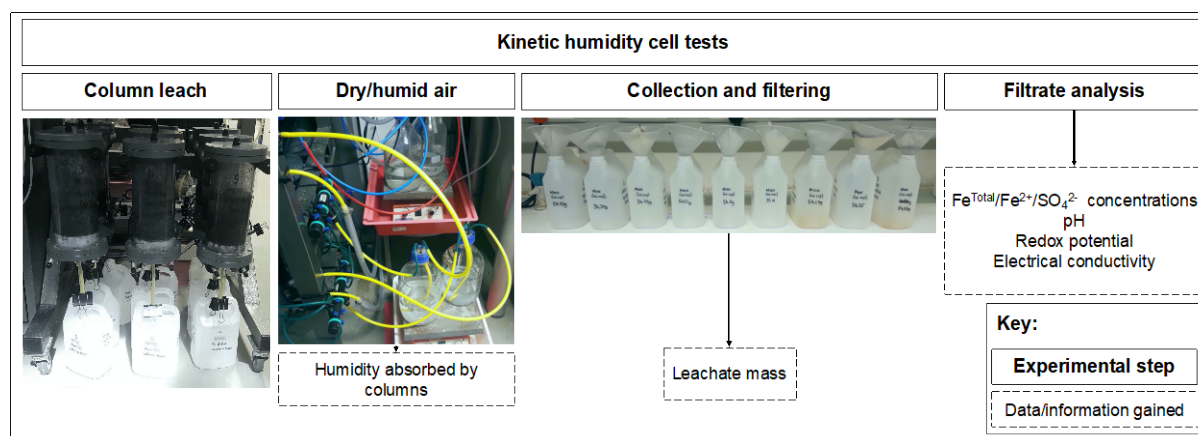


Figure 4-10 Humidity cell test set up

4.3.2 Sample characterisation

The water-fed humidity cell test (HCT) data are presented for 52 weeks for samples B and C and include the pH profiles, redox potential profiles, cumulative sulfate extraction profiles, and cumulative total iron extraction profiles. The ion concentrations are represented as cumulative extraction plots to provide an indication of the trend in leaching behaviour of the waste material over time, considering that the iron and sulfate concentrations were determined using methods that had a 0.01mg/L detection limit and 12% error on the iron (APHA, 1998) and sulfate (Moosa, 2000) concentrations, respectively. The pH and redox profiles are presented as the mean weekly values.

The water-fed pH profile of samples B and C showed a resulting circumneutral pH over the 52 weeks of the humidity cell test, even though the sulfide content was found to be 8.6% (predominantly pyrite) for sample B, and 31% (predominantly pyrrhotite) for sample C. These Fe-sulfide contents would lead to an expectation of acidic leachate formation; however, sample C also had a high calcite content (13%), which was higher than that of sample B (2.2%). Furthermore, from geochemical characterisation tests (Figure 3-7, section 3.3.1) sample B was classified as PAF (which should provide the largest

expectation of ARD generation), while sample C was uncertain due to both its high Fe-sulfide and dissolving (carbonate) mineral contents.

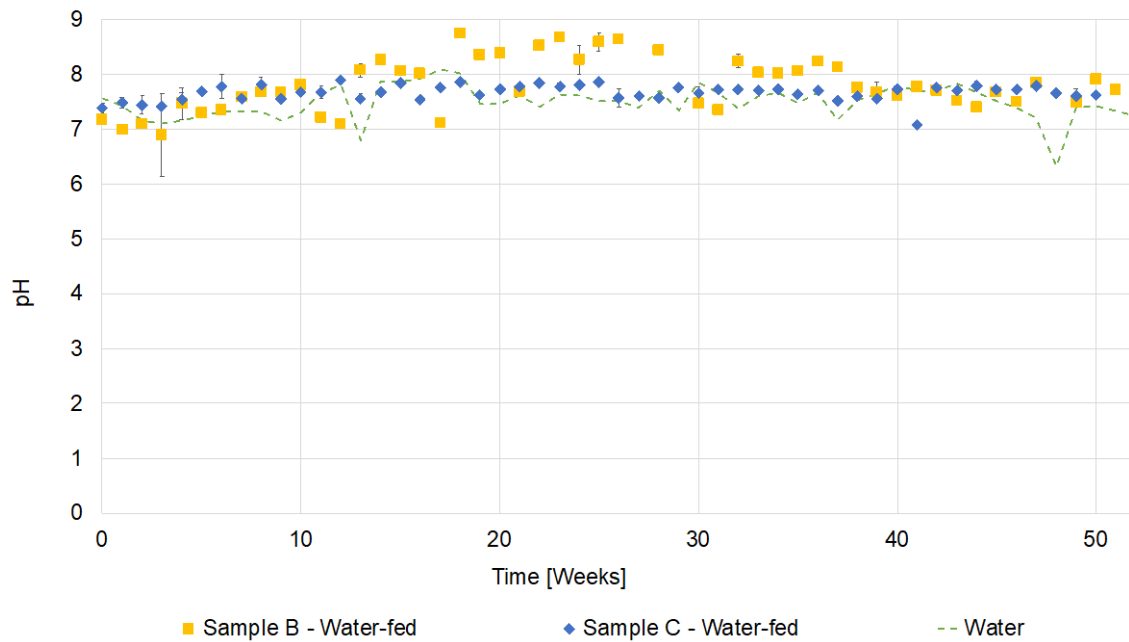


Figure 4-11 Water-fed humidity cell test pH profiles for samples B and C over the duration of 52 weeks. Data for sample B is sourced from the ongoing work of Opitz et al. (unpublished). The error reported is that obtained from 1x the standard deviation, which indicates the variation between the duplicate samples used in the test

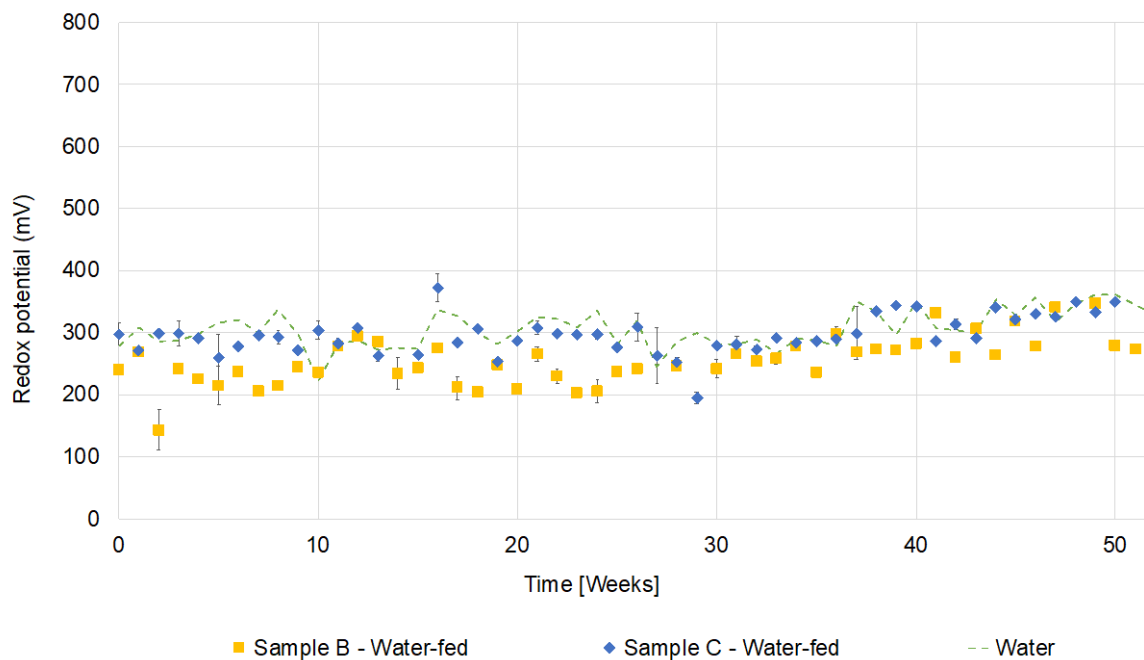


Figure 4-12 Water-fed humidity cell test redox potential profiles for samples B and C over the duration of 52 weeks. Data for sample B is sourced from the ongoing work of Opitz et al. (unpublished). The error reported is that obtained from 1x the standard deviation, which indicates the variation between the duplicate samples used in the test

The redox potential profile (Figure 4-12) was plotted to provide an indication of the relative abundance of the ferric and ferrous ions in solution, from which the microbial activity was inferred. Given the neutral pH conditions of the leachates, and the iron solubility at these levels, no (detectable) microbial activity was expected in the columns after 52 weeks (as similarly demonstrated by the UCT batch biokinetic test in section 3.3.2, Figure 3-11). This was confirmed by the water-fed column leachate redox potential remaining below 350mV for most weeks, with the remaining fluctuations largely being consistent with those of the de-ionised water feed, and thus not providing any indication of microbial activity.

The larger error bars on some data points (pH profile, Figure 4-11 – week 3 for sample B and redox potential profile, Figure 4-12 – weeks 2 and 14 for sample B and weeks 5, 16, 26 and 27 for sample C) may be attributed to a variety of factors. These include the possible deviation of the samples from one another due to sub-sampling errors, as well as due to the potential variation in the percolation channels or voids formed in the column, which would mean that the lixiviant could be contacting different minerals for the duration of the leach. Some reactive minerals (both acid-forming and neutralising), although potentially on the surface of the particles, could be in contact with other particles rather than the void spaces, as indicated by the high degree of association of dissolving and Fe-sulfide minerals in the largest size fractions (Figure 4-5 and Figure 4-8). It is expected that over time, as the reactive minerals would be leached, and the particle size decreased because of this, the void space arrangement in the column would change (Fagan-Endres et al., 2017; Ghorbani et al., 2011). These observations highlight some of the more commonly encountered problems associated with humidity cell tests that follow standard methods.

The sulfate and total iron concentrations were used to provide an indication of the leaching of Fe-sulfide material (predominantly pyrite for sample B and pyrrhotite for sample C) over the 52 weeks of the test. From Figure 4-13 (cumulative iron and sulfur extraction), the total iron and sulfate extractions increased minimally over the 52 weeks, with sulfate showing a greater percentage increase (0.97% for sample B and 1.7% for sample C) than iron, which was effectively zero. This low iron concentration in conjunction with the production of sulfate, especially for sample C may suggest Fe-sulfide dissolution, with the local formation of iron oxide/hydroxide precipitates in the columns due to the consistent high pH (mineralogical analyses could further be used to positively identify these precipitates but would necessitate the termination of the humidity cell test in order to do so). It should be noted that although the iron concentrations were low over the duration on the tests, Fe-sulfide dissolution may not be the only source of iron in solution over time as fast, intermediate and slow weathering iron-bearing minerals were present in the sample. Upon the formation of acidic leachate these minerals could dissolve and contribute to the ionic composition of the leachate. Sample B had only 22% of its iron hosted in sulfide minerals, with a larger component being found in magnetite (59%) and iron-bearing silicate minerals (18%), while for sample C the primary iron-bearing mineral was pyrrhotite, accounting for 89% of the total iron in the sample. Further details of the iron-distribution throughout the samples are given in the Supplementary Content section, Table A-5. The dissolution of iron-bearing silicates would also be accompanied by the deportment of other metals such as calcium, magnesium, aluminium and potassium.

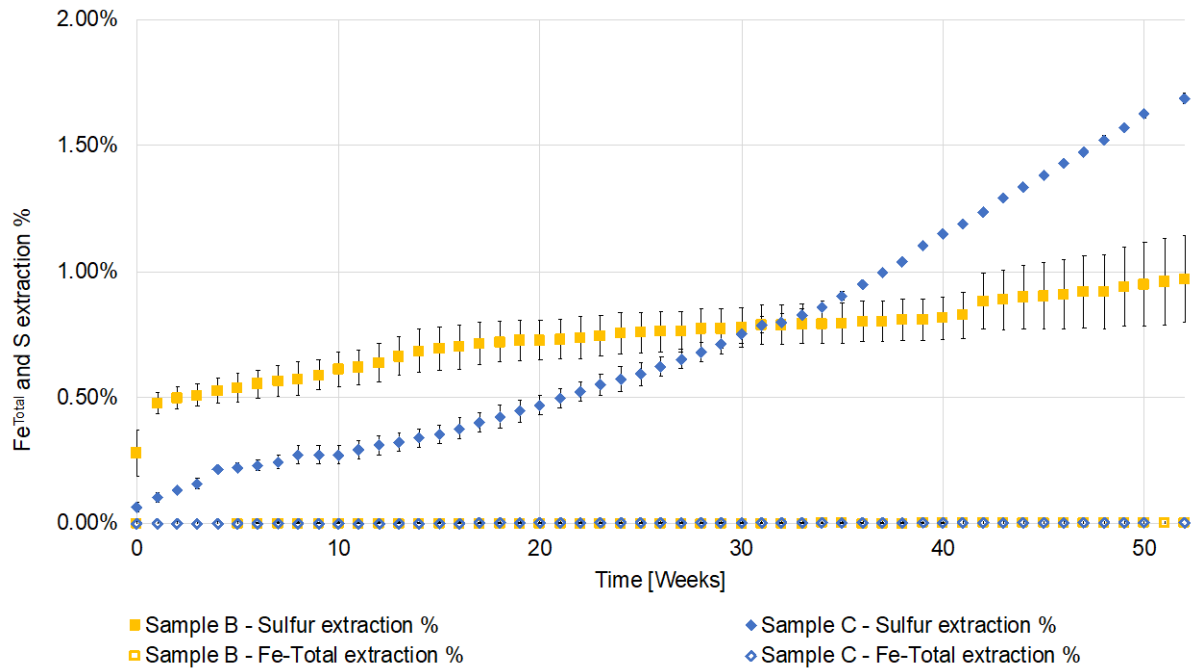


Figure 4-13 Cumulative total iron and sulfate extraction over the 52-week HCT test period for water-fed samples B and C. Error bars indicate 1x the standard deviation between replicate samples, which indicates the variation in concentration between the two replicate columns. It should be noted that the iron concentrations for the experiments was below the detection limit of 0.01mg/L for the assay method used to assess the iron concentration (APHA, 1998). Errors in sulfur extraction values do not include the 12% error previously reported for the barium chloride sulfate assay (APHA, 1995; Moosa, 2000)

5 The importance of mineralogy and texture in the ARD assessment “toolbox”

Overview: This chapter focuses on synthesising the results derived from the characterisation and prediction of ARD on the micro and meso scales in section 1 and 4, respectively using small scale laboratory tests coupled with quantitative mineralogy. The value derived from such an approach for ARD characterisation and prediction is also discussed. Two additional previously published international case studies using similar approaches to this study are collated here. Collective consideration of the three complementary data sets provides a strong evidence base to recommend the inclusion of quantitative mineralogical measurements into standard ARD characterisation and prediction protocols.

5.1 Synthesis of micro and meso scale ARD characterisation and prediction test results

On the micro scale, the static test results demonstrated that sample B was classified as potentially acid forming and sample C as uncertain. The use of quantitative mineralogy results confirmed this classification due to the greater content of Fe sulfide (8.6%, dominantly as pyrite) than dissolving mineral (2.2%) in sample B. Similarly, for sample C, the uncertain classification was confirmed through mineralogical analysis that indicated both a very high neutralising mineral (13%) and Fe-sulfide (31%, dominantly as pyrrhotite) content. The interpretation of the UCT batch biokinetic test results was similarly facilitated by consideration of both the compositions of the minerals present, and their relative grades. In this case, the presence of dissolving (carbonate) minerals in the non-pH controlled test pushed the pH to circumneutral, a regime unfavourable for the activity of the inoculum of mixed acidophilic microbes used in the test protocol. For the pH controlled batch biokinetic test results, consideration of the mineralogy allowed the interpretation of the relative contribution and rates of neutralising mineral dissolution. The interpretation, however, could still be further enhanced by analysis of the changes in the elemental composition of the leachate with time, and of the mineralogical changes of the solid residues with time (e.g. Becker et al., 2015; Opitz et al., 2018).

On the meso scale, the humidity cell test results demonstrated that after 52 weeks of the test, both samples B and C showed an absence of acidic leachate formation or microbial activity, despite the relatively high grades of Fe-sulfide minerals. Comparison of the Fe-sulfide liberation of the HCT feed material for samples B and C, showed that the former had a lower percentage of liberated Fe-sulfide material, with liberation only beginning in fractions below 2000 μ m. This was important to notice in conjunction with the PSD of the HCT feed material, as the majority of the mineral mass was found in the -6700/+2000 μ m size fraction, which exhibited the lowest degree of Fe-sulfide liberation for sample C and no liberation for sample B. This was shown by the generation of sulfate ions for sample C over the 52-week period of the test, which indicated some Fe-sulfide dissolution (more likely of the liberated Fe-sulfide grains). Nonetheless, the high degree of Fe-sulfide encapsulation in more than 50% of the material (based on the PSD) supported the absence of acidic leachate formation over the duration of the tests. Overall, the Fe-sulfide liberation increased as the size fraction decreased.

Considering the high degree of encapsulation/locking of the Fe-sulfide material it was important to consider the reactivity of the associated phases. The association for sample B was dominated by intermediate weathering, slow weathering and inert phases, while for sample C the association was dominated by inert and intermediate weathering minerals, with lesser association to slow weathering minerals. Greater association to dissolving minerals was found for sample C than sample B, which was attributed to the larger dissolving mineral content. The latter point may be important for the local

neutralisation potential available during humidity cell tests, which was emphasised by the association of unliberated dissolving minerals to Fe-sulfide minerals. The association to intermediate weathering phases may provide an indication that although the Fe-sulfide material was initially locked in other minerals, over time, if those minerals were to break down in an acidic environment, the Fe-sulfide minerals could become more liberated and subsequently begin contributing to ARD formation and drainage quality in the future.

A combination of the results from both the micro scale characterisation tests (static and UCT batch biokinetic) and meso scale characterisation and prediction tests (humidity cell) was central to the development of a more complete understanding of the ARD generating characteristics of the waste rock material as summarised in Figure 5-1.

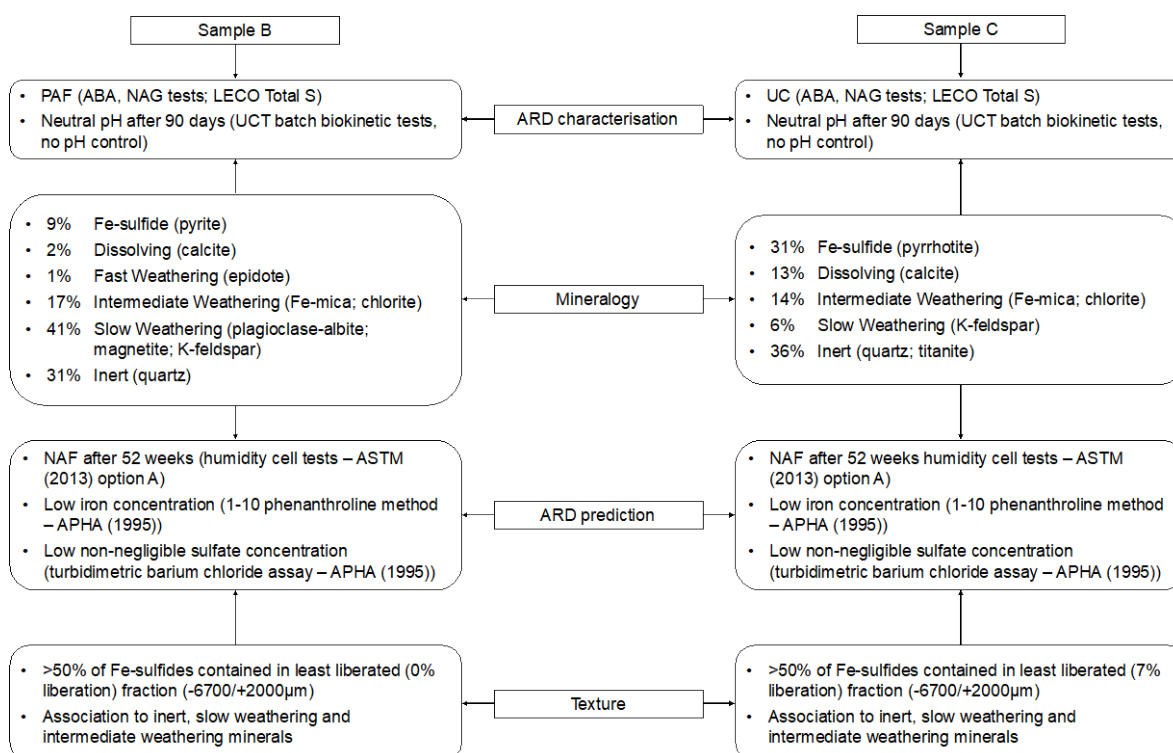


Figure 5-1 Summary of sample B and C characteristics, with arrows indicating the areas which they inform

5.2 Importance of mineralogy and texture on the interpretation of ARD prediction test results

The measurement of mineralogical data in terms of identifying the minerals present in the waste rock sample and their relevant quantities (also known as bulk mineralogy or mineral grades) provided certainty in the interpretation of the static test results. It also highlighted which sulfur-bearing minerals were present in the samples (e.g. pyrite, pyrrhotite and other sulfides, as well as knowledge of the sulfate species, if present) over and above the information provided by the total sulfur assay. This could also allow for the calculation of a mineralogical MPA, as opposed to the conventional MPA that assumes all sulfur present exists as pyritic sulfur (Weber et al., 2004b). The mineralogy similarly facilitated an understanding of the relative contribution of the different carbonates and silicate minerals to the acid neutralising capacity, given that fast and intermediate weathering silicate minerals may provide additional long term neutralising capacity (and themselves may partially contribute to the measured ANC determined using wet chemical analysis; Becker et al., 2015; Opitz et al., 2018). This knowledge is key for understanding the ARD characteristics on the micro scale, particularly for samples classifying as non-acid forming or uncertain (samples B and C in this study, respectively).



An important consideration in the interpretation of the laboratory scale static and batch biokinetic test results was that their interpretation was largely aided by the consideration of the mineralogy in terms of mineral grades alone and that the examination of their mineral liberation did not significantly alter the interpretation. This is because the Fe-sulfides in both samples were already generally liberated (94% and 71% liberated for sample B and C, respectively). This is consistent with how these tests have been designed to enable maximum sulfide and carbonate reactivity (Weber et al., 2005). Should liberation data be available, however, it can be used for the application of a liberation correction (sometimes also called a ‘locking correction’) as proposed by Brough et al. (2018) and Elghali et al. (2018). The liberation correction assumes that the static test results provide an overestimation of MPA for poorly liberated sulfides which are unlikely to contribute to the overall long term ARD generation, and a more representative corrected MPA can potentially be calculated if desired.

In contrast to the micro scale ARD testing the interpretation of the characterisation and prediction test results on the meso scale (humidity cell test) needed consideration of (i) mineral grades for the bulk sample, (ii) mineral distribution on a particle size-by-size basis and (iii) analysis of the liberation and association (locking) data for both the Fe-sulfides and dissolving minerals (carbonates). This knowledge was critical in understanding the behaviour of the HCT results where the leachate from both samples maintained a circumneutral pH over the 52-week duration of the test (Figure 4-10), even though both samples had a relatively high Fe-sulfide content. This was attributed to the fact that most of the Fe-sulfide sample mass (63% and 58% for samples B and C, respectively) occurred as unliberated Fe-sulfides associated with inert, slow and intermediate weathering silicate minerals within the coarser particle size fractions (>1mm; Figure 4-5). For these fractions the reaction rates are expected to be very slow due to the limited exposed of the reactive surface area. The very low levels of sulfur extraction (<2% for both samples; Figure 4-13) were most likely a result of minor oxidation of liberated Fe-sulfides in the finer size fractions where liberation was greatest (<150 µm; Figure 4-5 and Table 4-2). Similarly, although the majority of the dissolving minerals within both samples were largely unliberated and contained within particles of the coarser size fractions, rapid dissolution of small amounts of liberated carbonates within the finer size fractions and potentially the association of dissolving and Fe-sulfide minerals in larger size fractions ensured the circumneutral pH observed over the 52-week duration of the humidity cell tests.

Meso scale kinetic testing of waste rock material however, is specifically addressed at ARD prediction, whereby rates of ARD generation (including the lag time) and the net amount of acid that can be neutralised are estimated, as well as for modelling to predict the long-term impacts allowing for the recommendation of specific interventions to manage and mitigate ARD generation. In this case, knowledge of the mineral grades of the bulk samples, distribution of minerals on a particle size-by-size basis, as well as mineral liberation and association data is required to improve the certainty and accuracy of these mathematical models although such an approach to modelling (e.g. Simunika, 2013) has not been routinely applied to date.

To obtain representative and accurate mineralogical and textural data, it is critical to follow best practice. The following approach, which has been followed during this study, is supported by the abundant literature on process mineralogy measurements (e.g. Van der Plas & Tobi, 1965; Spencer & Sutherland, 2000; Evans & Morrison, 2016; Lotter, 2016; Wightman et al., 2016; Pooler & Dold, 2017; Bradshaw et al., 2019).

- Representative splitting and sub-sampling of the ‘as-received’ waste rock samples;
- Representative sub-sampling and size reduction during the preparation of material for micro scale (static and biokinetic) and meso scale (humidity cell) ARD characterisation and prediction testing;
- Mineralogy and texture measurements by auto-SEM-EDS technique (e.g. QEMSCAN, MLA, TIMA-X, Mineralogic) using samples prepared into polished resin blocks within discrete and

narrow size fractions. Methodological sample preparation processes are also critical to ensure a high-quality polish of the sample blocks with no plucking;

- Measurement of an adequate number of particles to ensure results are representative of the samples (i.e. through following strict sampling protocol rules, using tools like Gy's equation (François-Bongarçon and Gy, 2002; Gy, 2004) and assessing the number of measured particles and the associated errors involved through point counting (Van der Plas and Tobi, 1965; Evans and Napier-Munn, 2013) and/or estimation of confidence intervals (Leigh et al., 1993));
- Use of supporting mineralogical (e.g. QXRD) and chemical (e.g. LECO, XRF, ICP-OES, ICP-MS) analyses for the validation of the mineralogical results and to decrease measurement uncertainty. Ideally this should be done according to particle size fraction (for all, or at least a sub-set of the data) to minimise bias due to the settling of denser particles during the auto-SEM-EDS sample preparation procedures;
- Acknowledgement of the risk associated with stereological error during the measurements of liberation data from 2D sections. Typically, the greatest magnitude of stereological bias is associated with simple binary textures (unlike the very complex texture as seen in this study). Use of 3D X-ray computed tomography (XCT) scanning is a potential means of overcoming stereological error since a 3D volume of the particle is obtained. The XCT technique, however, suffers from lack of mineral discrimination (Bam et al., 2020). In this case, using XCT data would complement the mineral-textural results.

This study has focused the importance of mineralogy and texture in the interpretation of ARD characterisation and prediction test results. Within the scope of this work, 'mineralogy and texture' has been defined as 'knowing which minerals are present, their distribution on a particle size by size basis, as well as the mineral liberation and association/locking data (including knowledge of sulfide and carbonate mineral grain size distributions). In this work, minerals were grouped in terms of their weathering rates and the sulfides pyrite and pyrrhotite reported collectively as Fe-sulfides. This was done for simplicity and to facilitate comparison across samples with varying mineralogy. This approach of using such mineral groupings is not necessarily prescriptive and should be done at the discretion of those working with the data.

It should also be stressed, however, that in some cases a deeper and further investigation of metal liberation or metal deportment is also required, i.e. understanding the leaching of deleterious metals into solution as a consequence of sulfide oxidation, precipitation and redissolution (Hansen et al., 2008; Heikkinen et al., 2009; Plante et al., 2011; Opitz et al., 2016b). More specific analytical methods would be required to inform this level of understanding (and similarly the incorporation into the relevant models). This would encompass the use of analytical techniques such as electron probe micro-analysis (EPMA), and laser-ablation inductively coupled plasma mass spectrometry (LA-ICP-MS) in conjunction with sequential chemical extraction test work (also known as diagnostic leaching; Hansen et al., 2008).

5.3 A case study to support the recommendation for the integration of mineral textural information into the larger context of global protocol on ARD characterisation and prediction

The final objective of this study was to support the development of the recommendation for the integration of mineral textural information into the larger context of the global protocol on ARD characterisation and prediction. Review of the current accepted practice in the GARD guide indicates that "mineralogical testing is a required, not an optional, analysis". However, only visual descriptions of samples and simple petrographic analysis are required 'as a minimum' from which only a qualitative indication of which minerals are present and their mode of occurrence can be obtained. Additional means of mineralogical assessment are generally recommended, but not prescribed (INAP, 2009). The



ASTM test methods for humidity cells only ‘require’ measurement of mineral grades for the bulk sample, and quantification of the mineral distribution by size fraction, as well as liberation and association by size fraction is only ‘recommended’.

The number of arguments for the inclusion of mineralogy and texture into global protocol is increasingly growing stronger, as has been highlighted by recent review papers in the field (e.g. Parbhakar-Fox & Lottermoser, 2015; Dold, 2017); however, motivating for action based on these arguments ultimately requires a strong evidence base coming from independent studies. The results from this case study are summarised in Table 5-1 alongside the work of Brough et al. (2018) that presents two additional case studies from iron oxide-copper gold deposits in Australia and Scandinavia that have also undergone extensive characterisation and testing. The contributions of the Canadian case study (Elghali et al., 2018, 2019) is listed alongside, although their results were derived from column cell testing (that is not so explicitly regulated in terms of operating requirements). All these studies have systematically carried out mineral textural characterisation independently and have demonstrated the additional value that is obtained through this information.

Based on the findings from this evidence base covering a range of waste rock types, geographical region, climate, mineralogy and textural characteristics a case for the recommendation to incorporate mineralogy and texture measurements will be made. Ultimately it is proposed to collaboratively synthesise these results before approaching any international bodies. The recommendations are as follows:

- (a) For ARD characterisation – quantification of mineral grades (also known as bulk mineralogy or modal abundance) **is required** as part of the static ARD testing protocol since they provide more certainty to the classification. Quantitative measurements of sample material at the micro-scale provides additional useful information accompanying the static characterisation tests, particularly if the application of a liberation correction is desired, but this is considered supporting information rather than required information.
- (b) For ARD characterisation and prediction – quantification of mineral grades of the bulk sample (same as above), as well as quantification of mineral grades on a particle size-by-size basis accompanied by quantification of sulfide and carbonate mineral liberation and association **is required** as part of kinetic testing protocols of sample material on the meso-scale. This information is key to improving the certainty and accuracy of models for ARD generation allowing site specific predictions of the long terms impacts thus guiding the necessary interventions required.

Table 5-1 Summary of the case study data base intended to be used to motivate for the inclusion of mineral-textural information into standard global practice

Case study details					
	Case study 1 – this work		Case study 2 – Brough et al. (2018)	Case study 3 – Brough et al. (2018)	Case study 4 – Elghali et al. (2018, 2019)
	1B	1C			
Location	Africa		Australia	Scandinavia	Canada
Climate	Equatorial / tropical		Arid and hot	Arctic	Arctic-subarctic
Host ore type	Archean Orogenic gold (Greenstone belt)		Iron-oxide-copper gold (IOGC)	Iron-oxide-copper gold (IOGC)	Archean gold porphyry
Sulfide mineralogy	7.7 wt.% py <1 wt.% po	2.0 wt.% py 29.2 wt.% po	0.9 wt.% py <0.1 wt % other	1.7 wt% po 1.6 wt.% py 0.3 wt.% ccp < 0.1 wt.% other	0.3-2 wt.% py <0.1 wt.% other
Carbonate mineralogy	2.2 wt %	12.5 wt. %	0.3 wt. %	< 0.1 wt %.	Up to 8 wt. % in sample set
ARD characterisation on micro scale					
Static test classification	Potentially acid forming	Uncertain	Potentially acid forming	Potentially acid forming	Non-acid forming and uncertain
Fe-sulfide textures: Liberation and grain size	94% liberated, d ₅₀ 23 µm	71% liberated d ₅₀ 15 µm	-	-	
ARD characterisation and prediction on meso scale					
Kinetic tests	Stable pH ~7 after 52 weeks with some evidence of SO ₄ ²⁻ release in HCT tests	Stable pH ~7 after 52 weeks with some evidence of SO ₄ ²⁻ release in HCT tests	pH ~ 6.5 after 132 weeks with some evidence of SO ₄ ²⁻ release, negligible metal(loid) release in HCT tests	pH ~4 after 170 weeks with evidence of SO ₄ ²⁻ , Cu, Co, Zn and Ni release in HCT tests	Circumneutral pH after ~ 77 weeks with some evidence of SO ₄ ²⁻ , Cu and Zn release in column tests
Fe-sulfide textures: Liberation and grain size	14% liberated Fe-sulfides, d ₅₀ 118 µm. >50% of sample HCT mass in +2mm particle size fraction with 0% liberation	25% liberated Fe-sulfides, d ₅₀ 105 µm. >50% of sample HCT mass in +2mm particle size fraction with 7% liberation	2% liberated pyrite. 35% of sample HCT mass in +2mm particle size fraction with 0% liberation	36% liberated pyrite, 3.2% liberated pyrrhotite. 42% of sample HCT mass in +2mm particle size fraction with 0% liberation >50% of sample HCT mass in +2mm particle size fraction with 0% liberation	d ₅₀ of ~ 100µm. >80% of sample mass in +2mm particle size fraction with <10% liberation
Carbonate textures: Liberation and grain size	11% liberated with d ₅₀ of 55µm	16% liberated with d ₅₀ of ~ 65µm			d ₅₀ of ~ 50µm

6 Conclusions

Current methods and protocols for ARD assessment are not explicit in their requirement for mineralogical analysis but rather only recommended its usage. Typically, mineralogical and textural analyses are only incorporated if results of the ARD characterisation and prediction tests yield inadequate or conflicting information. The role of texture (and the individual textural parameters) in ARD formation is poorly understood. This is coupled with the difficulty in obtaining a representative sample for textural measurements, and in turn, a statistically sound, quantitative value for texture. Furthermore, the value of mineralogical and textural information for ARD assessment is rarely, if ever, weighed up against the end-of-the-line remediation and rehabilitation costs. Yet the accounts of the number of cases, and increasing costs associated with ARD management globally are numerous clearly indicating that the mining industry has still not yet successfully established a protocol that is wholly effective in mitigating and preventing ARD.

The overarching objective of this project is to quantitatively evaluate the role of mineralogy and texture in the context of commonly practiced ARD characterisation and prediction tests on both micro (<1mm) and meso (>1mm) scale material. Two waste rock samples (labelled sample B and C) derived from an African orogenic gold deposit have been studied extensively using a combination of standard static ARD characterisation tests (ABA, NAG, NAPP as well as the UCT batch biokinetic test) and kinetic humidity cell characterisation and prediction tests accompanied by detailed quantitative mineralogical analysis of particle mineral-textural properties using QEMSCAN (validated using a combination of QXRD and chemical assays).

6.1 Quantification of the effect of mineral texture on ARD characterisation at the micro scale

- Static ARD characterisation test results classified sample B as potentially acid forming and sample C as uncertain. Quantitative mineralogy results confirmed this classification due to the greater content of Fe sulfide (8.6%, dominantly as pyrite) than dissolving minerals (2.2%) in sample B. For sample C, the uncertain classification was confirmed through mineralogical analysis that indicated both a high neutralising mineral (13%) and Fe-sulfide (31%, dominantly as pyrrhotite) content.
- Batch biokinetic characterisation test results run under non pH-controlled conditions showed a circum-neutral pH profile for both samples within the first few days after the initiation of the test under acidic conditions. The circum-neutral pH was maintained for the duration of the 90-day test. This was attributed to the dissolution of minor liberated carbonates that raised the pH into a regime unfavourable for microbial activity. However, once the neutralising capacity had been depleted (pH-controlled test), sample C did ultimately maintain acidic conditions (attributed to microbially mediated oxidation of liberated sulfides).
- The mineral textural characteristics of both samples at the micro-scale (both samples were prepared to >90% passing 150 µm) fall into a liberation-dominated textural regime (Fe-sulfide liberation > 70% for both samples, $d_{50} \sim 20\mu\text{m}$) and are consistent with the standard characterisation tests providing an indication of the 'worst point scenario' of ARD generation. Quantification of the liberation characteristics did not change the interpretations of the characterisation test results but rather provided more certainty and accuracy to the waste rock classification.

6.2 Quantification of the effect of mineral texture on ARD characterisation and prediction at the meso scale

- Kinetic characterisation and prediction (humidity cell) tests results remained circumneutral in pH over 52 weeks and showed an absence of acidic leachate formation. Only very minor Fe-sulfide dissolution occurred despite the relatively high grades of Fe-sulfide minerals (8.6% and 31% Fe-sulfides for samples B and C, respectively).
- The lack of acidic leachate generation was attributed to a combination of the following mineral texture factors: over 50% of the sample mass of Fe-sulfides occurred in the +1mm size fractions that showed negligible liberation (surface exposure) resulting in a net Fe-sulfide liberation of 14% (sample B) and 25% (sample C); overall carbonate mineral liberation was similarly low (between 11% and 16%); unliberated Fe-sulfide and carbonate minerals in both samples showed strong associations to intermediate weathering, slow weathering and inert minerals.
- The mineral textural characteristics of both samples on the meso scale (>1mm) fell into an association (locking) dominated textural regime due to the high degree of Fe-sulfide encapsulation in the bulk of the material. Measurement of Fe-sulfide grain size distributions similarly supported these findings ($d_{50} \sim 110 \mu\text{m}$). Quantification of the liberation characteristics was critical to the interpretation of the test results and provided more certainty and accuracy to the waste rock characterisation.

6.3 Integrating quantitative mineral texture measurements into the ARD characterisation protocol for improved accuracy in ARD characterisation and prediction

- A combination of the results from both the micro scale characterisation tests (static and UCT batch biokinetic) and meso scale characterisation and prediction tests (humidity cell) alongside quantitative mineral-textural analyses was central to the development of a more complete understanding of the ARD generating characteristics of the waste rock material, i.e. mineralogical and static tests indicated sample B as potentially acid forming and sample C as uncertain whereas 52 weeks of humidity cell kinetic testing indicated an absence of acidic leachate due to the extensive lag time for ARD generation primarily given the very low degrees of sulfide liberation. This provides more certainty and accuracy to waste rock classification and modelling of the long term ARD generating properties. This in turn allows site specific predictions of the long terms impacts thus ultimately guiding the necessary interventions required.
- The acquisition of mineralogy and textural measurements should follow best practice with respect to sampling, sample preparation, measurement, data processing and validation to obtain meaningful, representative and accurate mineral-texture data.
- A variety of additional mineralogical measurement types exist that have not been investigated in detail in this study since they fall outside of the scope of this project; however, these aspects are still important within the broader ARD characterisation and prediction practice – for example the spatial measurement of trace element compositions of pyrite using a technique such as laser-ablation ICP-MS to further understand the deportment of deleterious elements.
- This work has developed an African case study to recommend that mineral textural information is a critical component of the ARD characterisation and testing protocol and its integration into standard international testing protocol is required. Alongside the African case study, three additional independent case studies have been highlighted in the literature representing waste rock studies from Canada, Australia and Scandinavia spanning a variety of waste rock types (including differing mineralogy and texture), as well as climate (Brough et al., 2018; Elghali et



al., 2018, 2019). Collectively these four case studies provide a strong evidence base on which the international agency can be approached.

6.4 Recommendations

- Quantification of mineral grades (also known as bulk mineralogy or modal abundance) is required as part of the static ARD characterisation testing protocol since the information provides certainty to waste rock classification. Quantitative mineral texture measurements of this material provides additional information accompanying the static characterisation tests (particularly if the application of a liberation correction is desired), but this represents supporting information rather than required information.
- Quantification of (i) mineral grades (also known as bulk mineralogy or modal abundance), (ii) mineral grade on a particle size-by-size basis (also known as mineral distribution by size) and (iii) sulfide and carbonate mineral liberation and association on a particle size-by-size basis is required as part of the kinetic ARD characterisation and prediction testing protocol. This information is key to improving the certainty and accuracy of models for ARD generation allowing site specific predictions of the long terms impacts thus guiding the necessary interventions required.
- The results of this study are collectively collated with those of three other published international case studies as a representative and strong evidence base to recommend the prescription of mineral textural information into the larger context of local and global protocol on ARD characterisation and prediction.

References

- Akcil A, Koldas S (2006) Acid Mine Drainage (AMD): causes, treatment and case studies. *J Clean Prod* 14:1139-1145.
- APHA (1999) Standard Methods for the Examination of Water and Wastewater – Inorganic Metals, Organics, Oxygen, Carbon, Humics, DBPs. 733
- APHA (1998) Standard methods for the examination of water and wastewaters. American Public Health Association 20th Edition. Washington, DC
- APHA (1995) Standard methods for the examination of water and wastewaters. American Public Health Association 19th Edition. Washington, DC
- ASTM (2013) Standard Test Method for Laboratory Weathering of Solid Materials Using a Humidity Cell. D5744-13 1-23.
- Bam LC, Miller JA, Becker M (2020) A Mineral X-ray Linear Attenuation Coefficient Tool (MXLAC) to Assess Mineralogical Differentiation for X-ray Computed Tomography Scanning. *Minerals* 10:441.
- Becker M, Dyantyi N, Broadhurst JL, Harrison STL, Franzidis JP (2015) A mineralogical approach to evaluating laboratory scale acid rock drainage characterisation tests. *Miner Eng* 80:33-36.
- Becker M, Wightman EM, Evans CL (eds) (2016) Process Mineralogy: JKMRC Monograph Series in Mining and Mineral Processing: No. 6. Julius Kruttschnitt Mineral Research Centre, The University of Queensland, Queensland, Australia
- Bowen NL (1922) The Reaction Principles in Petrogenesis. *J Geol* 30:177-198.
- Bradshaw D, Wilkie G, Becker M, Evans C, Lotter N (2019) Ore Liberation Analysis. In: Dunne RC, Komar Kawatra S, Young CA (eds) SME Mineral Processing & Extractive Metallurgy Handbook, Volume One & Two. Society for Mining, Metallurgy & Exploration, Englewood, Colorado, USA, pp 69-88
- Broadhurst JL, Bryan CG, Becker M, Franzidis JP, Harrison STL (2013) Characterising the Acid Generating Potential of Mine Wastes by means of Laboratory-scale Static and Biokinetic Tests. In: Wolkersdorfer, Brown, Figueroa (eds) International Mine Water Association Annual Conference: International Mine Water Association. pp 275-280
- Brough C, Strongman J, Howell R, Warrender R, Prestia A, Barnes A, Fletcher J (2017) Automated environmental mineralogy; the use of liberation analysis in humidity cell testwork. *Miner Eng* 107:112-122.
- Brough C, Strongman J, Fletcher J, Garner C, Parbhakar-Fox A, Barnes A, Howell R, Griffiths R (2018) Automated environmental mineralogy; using image processing tools to maximise the efficient analysis of liberation across multiple size fractions. In: Process Mineralogy '18. Cape Town
- Brough CP, Warrender R, Howell RJ, Barnes A, Parbhakar-Fox A (2013) The process mineralogy of mine wastes. *Miner Eng* 52:125-135.
- Bruker AXS GmbH (2008) TOPAS 4 User Manual
- Bruynesteyn A, Hackl RP (1982) Evaluation of acid production potential of mining waste materials. *Miner Environ* 4:5-8.
- Bryan CG (2006) A study of the microbiological populations of mine wastes. PhD Thesis. University of Wales, Bangor
- Carrasco P, Carrasco P, Jara E (2004) The economic impact of correct sampling and analysis practices in the copper mining industry. *Chemom Intell Lab Syst* 74:209-213.

- Columbia Center on Sustainable Investment, Sustainable Development Solutions Network, UNDP, World Economic Forum (2016) Mapping mining to the sustainable development goals: A preliminary atlas (executive summary)
- Cozzolino D, Chandra S, Roberts J, Power A, Rajapaksha P, Ball N, Gordon R, Chapman J (2018) There is gold in them hills: Predicting potential acid mine drainage events through the use of chemometrics. *Sci Total Environ* 619-620:1464-1472.
- Dold B (2017) Acid rock drainage prediction: A critical review. *J Geochemical Explor* 172:120-132.
- Dyantyi N, Becker M, Broadhurst JL, Harrison STL, Franzidis JP (2013) Use of mineralogy to interpret laboratory-scale acid rock drainage prediction tests – A gold case study. In: *World Gold 2013. The Australasian Institute of Mining and Metallurgy, Melbourne*, pp 519-526
- Elghali A, Benzaazoua M, Bouzahzah H, Bussière B, Villarraga-Gómez H (2018) Determination of the available acid-generating potential of waste rock, part I: Mineralogical approach. *Appl Geochemistry* 99:31-41.
- Elghali A, Benzaazoua M, Bussière B, Bouzahzah H (2019) Determination of the available acid-generating potential of waste rock, part II: Waste management involvement. *Appl Geochemistry* 100:316-325.
- Evans C (2010) Development of a methodology to estimate flotation separability from ore microtexture. Sustainable Minerals Institute, PhD Thesis. University of Queensland
- Evans CL, Morrison RD (2016) Mineral Liberation. In: Becker M, Wightman EM, Evans CL (eds) *Process Mineralogy: JKMRM Monograph Series in Mining and Mineral Processing: No. 6*. pp 219-233
- Evans CL, Napier-Munn TJ (2013) Estimating error in measurements of mineral grain size distribution. *Miner Eng* 52:198-203.
- Fagan-Endres MA, Cilliers JJ, Sederman AJ, Harrison STL (2017) Spatial variations in leaching of a low-grade, low-porosity chalcopyrite ore identified using X-ray μ CT. *Miner Eng* 105:63-68.
- François-Bongarçon D, Gy P (2002) The most common error in applying “Gy’s formula” in the theory of mineral sampling, and the history of the liberation factor. *J South African Inst Min Metall* 102:475-479
- Gay SL (2004) Simple texture-based liberation modelling of ores. *Miner Eng* 17:1209-1216.
- Ghorbani Y, Becker M, Mainza A, Franzidis JP, Petersen J (2011) Large particle effects in chemical/biochemical heap leach processes – A review. *Miner Eng* 24:1172-1184.
- Ghorbani Y, Becker M, Petersen J, Mainza AN, Franzidis JP (2013) Investigation of the effect of mineralogy as rate-limiting factors in large particle leaching. *Miner Eng* 52:38-51.
- Golela MT, Ntwampe SKO, Harrison STL (2018) Effect of Microbial Consortium on the Biokinetic Test for Assessing Acid Rock Drainage Potential. MSc Thesis. Cape Peninsula University of Technology
- Gu Y, Schouwstra RP, Rule C (2014) The value of automated mineralogy. *Miner Eng* 58:100-103.
- Gy P (1979) Chapter 26 – Practical Implementation of Splitting Processes – Example – Reduction of Drill Core Samples. In: *Developments in Geomathematics*. Amsterdam, pp 311-321
- Gy P (2004) Sampling of discrete materials – A new introduction to the theory of sampling: I. Qualitative approach. *Chemom Intell Lab Syst* 74:7-24.
- Hallberg KB (2010) New perspectives in acid mine drainage microbiology. In: *Hydrometallurgy*. pp 448-453
- Hansen Y, Broadhurst JL, Petrie JG (2008) Modelling leachate generation and mobility from copper sulphide tailings – An integrated approach to impact assessment. *Miner Eng* 288-301



- Heikkinen P, Räisänen M, Johnson R (2009) Geochemical characterisation of seepage and drainage water quality from two sulphide mine tailings impoundments: acid mine drainage versus neutral mine drainage. *Mine Water Environ* 28:30-49
- Hesketh AH, Broadhurst JL, Bryan CG, Van Hille RP, Harrison STL (2010) Biokinetic test for the characterisation of AMD generation potential of sulfide mineral wastes. *Hydrometallurgy* 104:459-464.
- INAP (2009) The International Network for Acid Prevention (INAP). Global Acid Rock Drainage Guide (GARD Guide)
- Jambor JL, Dutrizac JE, Raudsepp M (2007) Measured and computed neutralization potentials from static tests of diverse rock types. *Environ Geol* 52:1019-1031.
- Jamieson HE, Walker SR, Parsons MB (2015) Mineralogical characterization of mine waste. *Appl Geochemistry* 57:85-105.
- Jardine MA, Miller JA, Becker M (2018) Computers and Geosciences Coupled X-ray computed tomography and grey level co-occurrence matrices as a method for quantification of mineralogy and texture in 3D. *Comput Geosci* 111:105-117.
- Jennings SR, Dollhopf DJ (1995) Acid-base account effectiveness for determination of mine waste potential acidity. *J Hazard Mater* 41:161-175.
- Kocabag D (1985) The effect of grinding media and galvanic interactions upon the flotation of sulfide minerals. In: *Complex Sulfides, Process Symposium 5*. pp 81-97
- Komadel P, Stucki JW (1988) Quantitative assay of minerals for Fe²⁺ and Fe³⁺ using 1,10-phenanthroline: iii. A rapid photochemical method. *Clays Clay Miner* 36:379-381.
- Kwong JYT (1993) Prediction and prevention of acid rock drainage from a geological and mineralogical perspective; MEND Project 1.32.1. Saskatchewan, Canada
- Lapakko K (2002) Metal mine rock and waste characterization tools: An overview. *Int Inst Environ Dev* 2002
- Lapakko K, Antonson DA (2006) Pyrite Oxidation Rates From Humidity Cell Testing of Greenstone Rock
- Lätti D, Adair BJI (2001) An assessment of stereological adjustment procedures. *Miner Eng* 14:1579-1587.
- Lawrence RW, Scheske M (1997) A method to calculate the neutralization potential of mining wastes. *Environ Geol* 32:100-106.
- Leigh GM, Sutherland DN, Gottlieb P (1993) Confidence limits for liberation measurements. *Miner Eng* 6:155-161.
- Lengke MF, Davis A, Bucknam C (2010) Improving management of potentially acid generating waste rock. *Mine Water Environ* 29:29-44.
- Lotter NO (2016) Sampling for Process Mineralogy. In: Becker M, Wightman E., Evans C. (eds) *Process Mineralogy: JKMRC Monograph Series in Mining and Mineral Processing: No. 6*. Julius Kruttschnitt Mineral Research Centre, The University of Queensland, pp 7-20
- Lottermoser BG (2010) *Mine Wastes: Characterization, treatment and environmental impacts*, 3rd edn. Springer, Berlin
- Maest AS, Nordstrom DK (2017) A geochemical examination of humidity cell tests. *Appl Geochemistry* 81:109-131.
- Mainza AN, Powell MS (2016) Particle Size Analysis. In: *Process Mineralogy: JKMRC Monograph Series in Mining and Mineral Processing: No. 6*. Julius Kruttschnitt Mineral Research Centre, The University of Queensland, pp 21-35

- Makaula DX, Huddy RJ, Fagan-Endres MA, Harrison STL (2018) Developing a Flow-Through Biokinetic Test to Characterize ARD Potential: Investigating the Microbial Metabolic Activity on Pyrite-bearing Waste Rock Surfaces in an Unsaturated Ore Bed. In: Wolkersdorfer C, Sartz L, Weber A, Burgess J, Tremblay G (eds) 11th ICARD | IMWA | MWD Conference. pp 399-405
- McCarthy TS (2011) The impact of acid mine drainage in South Africa. *S Afr J Sci* 107:1-7.
- Miller JD, Lin CL, Hupka L, Al-Wakeel MI (2009) Liberation-limited grade/recovery curves from X-ray micro CT analysis of feed material for the evaluation of separation efficiency. *Int J Miner Process* 93:48-53.
- Miller S, Robertson A, Donahue T (1997) Advances in Acid Drainage Prediction Using the Net Acid Generation (NAG) Test. In: 4th International Conference on Acid Rock Drainage. Vancouver, pp 533-549
- Moncur MC, Jambor JL, Ptacek CJ, Blowes DW (2009) Mine drainage from the weathering of sulfide minerals and magnetite. *Appl Geochemistry* 24:2362-2373.
- Moosa S (2000) A kinetic study on anaerobic sulphate reduction: effects of sulphate and temperature. PhD Thesis. University of Cape Town
- Morin KA, Hutt NM (2001) Environmental geochemistry of minesite drainage: practical theory and case studies
- Morin KA, Hutt NM (1998) Kinetic tests and risk assessment for ARD. In: 5 Annual BC Metal Leaching and ARD Workshop
- Nordstrom DK, Alpers CN (1999) Geochemistry of acid mine waters. *Environ Geochemistry Miner Depos* 6:133-160
- Opitz AKB, Becker M, Broadhurst JL, Bradshaw DJ, Harrison STL (2016a) The Biokinetic Test as a Geometallurgical Indicator for Acid Rock Drainage Potentials. Perth, Australia, pp 183-191
- Opitz AKB, Becker M, Harrison STL, Broadhurst JL (2016b) Characterising Environmental Risks Associated with Sulfide-bearing Gold Wastes. In: International Mine Water Association: Mining Meets Water – Conflicts and Solutions. pp 1050-1057
- Opitz AKB, Broadhurst JL, Harrison STL, Bradshaw DJ, Becker M (2018) Understanding Mineralogy As A Tool For Acid Rock Drainage Characterisation. In: Wolkersdorfer C, Sartz L, Weber A, Burgess J, Tremblay G (eds) 11th International MineWater Association/International Conference for Acid Rock Drainage (11th ICARD | IMWA |MWD2018). Mine Water – Risk to Opportunity (Vol I). pp 424-429
- Opitz AKB, Guseva O, Harrison STL, Broadhurst JL, Becker M (Unpublished) Modification of feed acidity and irrigation schemes for a reduction in humidity cell test duration
- Opitz AKB, Harrison STL, Broadhurst JL, Becker M (2020) A systematic approach for the assessment of environmental hazards associated with acid rock drainage (ARD) generation. Unpublished manuscript.
- Paktunc AD (1999) Mineralogical constraints on the determination of neutralization potential and prediction of acid mine drainage. *Environ Geol* 39:103-112.
- Parbhakar-Fox A (2012) Establishing the value of an integrated geochemistry-mineralogy-texture approach for acid rock drainage prediction. PhD Thesis. University of Tasmania
- Parbhakar-Fox A, Edraki M, Walters S, Bradshaw D (2011) Development of a textural index for the prediction of acid rock drainage. *Miner Eng* 24:1277-1287.
- Parbhakar-Fox A, Lottermoser B, Bradshaw D (2013) Evaluating waste rock mineralogy and microtexture during kinetic testing for improved acid rock drainage prediction. *Miner Eng* 52:111-124.



- Parbhakar-Fox A, Lottermoser BG (2015) A critical review of acid rock drainage prediction methods and practices. *Miner Eng* 82:107-124.
- Pérez-Barnuevo L, Pirard E, Castroviejo R (2013) Automated characterisation of intergrowth textures in mineral particles. A case study. *Miner Eng* 52:136-142.
- Petersen L, Dahl CK, Esbensen KH (2004) Representative mass reduction in sampling – A critical survey of techniques and hardware. *Chemom Intell Lab Syst* 74:95-114.
- Petersen L, Minkinen P, Esbensen KH (2005) Representative sampling for reliable data analysis: Theory of Sampling. *Chemom Intell Lab Syst* 77:261-277.
- Plante B, Benzaazoua M, Bussière B (2011) Predicting Geochemical Behaviour of Waste Rock with Low Acid Generating Potential Using Laboratory Kinetic Tests. *Mine Water Environ* 30:2-21.
- Plumlee GS (1999) The Environmental Geology of Mineral Deposits. In: *Reviews in Economic Geology*. pp 71-116
- Pooler R, Dold B (2017) Optimization and Quality Control of Automated Quantitative Mineralogy Analysis for Acid Rock Drainage Prediction. *Minerals* 7:12.
- Schippers A, Glombitza F, Sand W (2014) *Geobiotechnology I Metal-related Issues*. Springer
- Simunika NN (2013) Predicting the time related generation of acid rock drainage from mine waste: a copper case study. MSc Thesis. University of Cape Town
- Smart R, Skinner B, Levay G, Gerson A, Thomas J, Sobobieraj H, Schumann R, Weisener C, Weber P, Miller S, Stewart W (2002) ARD test handbook: Project P387A prediction and kinetic control of acid mine drainage. Proj P387A, Predict Kinet Control acid mine Drain 42
- Spencer S, Sutherland DN (2000) Stereological correction of mineral liberation grade distributions estimated by single sectioning of particles. *Image Anal Stereol* 19:175-182.
- Stewart WA, Miller SD, Smart R (2006) Advances in Acid Rock Drainage (Ard) Characterisation of Mine Wastes. *J Am Soc Min Reclam* 2006:2098-2119.
- Strotzki W (2010) Introduction to texture analysis: macrotexture, microtexture and orientation mapping. *J Appl Crystallogr* 43:947
- Sverdrup H (1990) *The kinetics of chemical weathering*. Lund University Press, Lund, Sweden and Chartwell-Bratt Ltd, London
- Ueda T, Oki T, Koyanaka S (2016) Stereological bias for spherical particles with various particle compositions. *Adv Powder Technol* 27:1828-1838.
- Ueda T, Oki T, Koyanaka S (2017) Stereological correction method based on sectional texture analysis for the liberation distribution of binary particle systems. *Adv Powder Technol* 28:1391-1398.
- Ueda T, Oki T, Koyanaka S (2018) A general quantification method for addressing stereological bias in mineral liberation assessment in terms of volume fraction and size of mineral phase. *Miner Eng* 119:156-165.
- Van der Plas LVD, Tobi AC (1965) A chart for judging the reliability of point counting results. *Am J Sci* 263:87-90
- Vera M, Schippers A, Sand W (2013) Progress in bioleaching: Fundamentals and mechanisms of bacterial metal sulfide oxidation-part A. *Appl. Microbiol. Biotechnol.* 97:7529-7541
- Vos F (2017) The effect of mineral grain textures at particle surfaces on flotation response. PhD Thesis. University of Queensland
- Weber PA, Stewart WA, Skinner WM, Weisener CG, Thomas JE, Smart RSC (2004a) Geochemical effects of oxidation products and framboidal pyrite oxidation in acid mine drainage prediction techniques. *Appl Geochemistry* 19:1953-1974.

- Weber PA, Thomas JE, Skinner WM, Smart RSC (2004b) Improved acid neutralisation capacity assessment of iron carbonates by titration and theoretical calculation. *Appl Geochemistry* 19:687-694.
- Weber PA, Thomas JE, Skinner WM, Smart RSC (2005) A methodology to determine the acid-neutralization capacity of rock samples. *Can Mineral* 43:1183-1192
- White W, Lapakko K, Cox R (1997) The Environmental geochemistry of mineral deposits. Part A. Processes, methods and health Issues. *Rev Econ Geol* 6:325-338
- Wightman EM, Evans CL (2014) Representing and interpreting the liberation spectrum in a processing context. *Miner Eng* 61:121-125.
- Wightman EM, Evans CL, Becker M, Gu Y (2016) Automated Scanning Electron Microscopy with Energy Dispersive Spectrometry. In: Becker M, Wightman EM, Evans CL (eds) *Process Mineralogy: JKMRC Monograph Series in Mining and Mineral Processing: No. 6*. Julius Kruttschnitt Mineral Research Centre, The University of Queensland, pp 97-107



Supplementary content

The supplementary electronic content of this project is available at:

<https://doi.org/10.25375/uct.12377129>.

Table A-1 XRF data for samples B and C

Sample		B	C			B	C
SiO₂	wt. %	54	41	Y	(ppm)	94	1979
TiO₂	wt. %	0.2	1.7	Sr	(ppm)	54	312
Al₂O₃	wt. %	8.9	7.4	Rb	(ppm)	248	317
Fe₂O₃	wt. %	18	19	U	(ppm)	52	5.8
MnO	wt. %	0.1	0.3	Th	(ppm)	6.0	20
MgO	wt. %	1.6	3.3	Pb	(ppm)	103	148
CaO	wt. %	2.7	9.9	Co	(ppm)	15	24
Na₂O	wt. %	3.0	0.1	Mn	(ppm)	596	138
K₂O	wt. %	2.6	2.0	Cr	(ppm)	84	58
P₂O₅	wt. %	0.1	0.2	V	(ppm)	b.d.	<5
SO₃	wt. %	1.2	15	F	(ppm)	2.1	<5
Cr₂O₃	wt. %	0.1	0.2	S	(ppm)	23	50
NiO	wt. %	0.1	<0.1	Cl	(ppm)	17	118
H₂O-	wt. %	4.2	n.a.	Sc	(ppm)	627	2470
LOI	wt. %	3.1	n.a.	Ba	(ppm)	687	1118
Sum	wt. %	100	99	Zn	(ppm)	66	252
				Cu	(ppm)	1194	1458
				Ni	(ppm)	7667	19120
				Mo	(ppm)	266	126
				Nb	(ppm)	6.3	39
				Zr	(ppm)	648	478

Table A-2 Bulk mineralogy for samples B and C as determined using quantitative XRD

Mineral	Sample B	Sample C
Pyrite	6.8%	<1%
Pyrrhotite	<1%	26.8%
Other Sulfide	<1%	<1%
Carbonate	4.9%	16.7%
Olivine	<1%	<1%
Epidote	2.2%	2.5%
Pyroxene	<1%	<1%
Amphibole	1.8%	<1%
Mica	8.7%	<1%
Chlorite	2.2%	6.0%
Talc	<1%	<1%
Plagioclase-Feldspar	24.1%	<1%
K-Feldspar	7.3%	2.7%
Fe-Oxide	8.1%	<1%
Quartz	33.0%	37.4%
Titanite	<1%	7.1%
Apatite	<1%	<1%
R_{wp}	8.21	6.62
GOF	4.56	2.10

Table A-3 Sized mineralogy for samples B as determined using QEMSCAN

Mineral group	Size fraction (µm)					Combined
	-6700/+2000	-2000/+1000	-1000/+425	-425/+150	-150/+0	
Pyrite	4.8	0.9	0.4	0.5	0.5	7.1
Pyrrhotite	0.6	0.1	<0.1	0.1	0.1	0.9
Other Sulfide	<0.1	<0.1	<0.1	<0.1	<0.1	<0.1
Carbonate	2.4	0.5	0.3	0.4	0.3	3.8
Olivine	0.3	0.1	<0.1	<0.1	<0.1	0.5
Epidote	0.1	<0.1	<0.1	<0.1	<0.1	0.2
Pyroxene	0.4	0.2	0.1	0.1	<0.1	0.8
Amphibole	2.9	0.7	0.3	0.4	0.3	4.6
Mica	5.8	0.8	0.5	0.9	0.6	8.6
Chlorite	1.0	0.2	0.1	0.1	0.1	1.6
Plagioclase-Feldspar	<0.1	<0.1	<0.1	<0.1	<0.1	<0.1
K-Feldspar	12.6	2.5	1.3	2.3	1.5	20.2
Fe-Oxide	6.0	1.2	0.6	1.0	0.7	9.6
Quartz	4.6	1.0	0.5	0.6	0.4	7.0
Titanite	21.3	4.3	2.1	3.6	2.1	33.4
Other	<0.1	<0.1	<0.1	<0.1	<0.1	<0.1

Table A-4 Sized mineralogy for samples C as determined using QEMSCAN

Mineral group	Size fraction (µm)					Combined
	-6700/+2000	-2000/+1000	-1000/+425	-425/+150	-150/+0	
Pyrite	0.2	0.1	<0.1	<0.1	0.2	0.5
Pyrrhotite	15.8	4.5	2.9	1.3	4.4	28.9
Other Sulfide	0.2	0.1	<0.1	<0.1	0.1	0.4
Carbonate	6.7	1.5	1.6	0.6	2.3	12.7
Olivine	<0.1	<0.1	<0.1	<0.1	<0.1	<0.1
Epidote	0.1	<0.1	<0.1	<0.1	<0.1	0.2
Pyroxene	0.2	<0.1	<0.1	<0.1	<0.1	0.3
Amphibole	0.3	0.1	0.2	<0.1	<0.1	0.6
Mica	4.6	1.0	0.7	0.2	0.7	7.2
Chlorite	2.1	0.5	0.5	0.2	0.5	3.7
Plagioclase-Feldspar	<0.1	<0.1	<0.1	<0.1	<0.1	<0.1
K-Feldspar	0.1	<0.1	<0.1	<0.1	<0.1	0.2
Fe-Oxide	3.1	0.6	0.7	0.2	0.5	5.1
Quartz	<0.1	<0.1	0.1	<0.1	<0.1	0.2
Titanite	19.5	4.2	3.9	1.5	2.4	31.4
Other	3.4	0.7	0.6	0.2	0.4	5.3

Texture Measurements into the ARD Characterisation Protocol for Improved Accuracy in ARD Characterisation and Prediction

Table A-5 Distribution of iron across the minerals in samples B and C as a percentage of the total iron in the sample. This was obtained using the Electron Probe Microanalysis (EPMA) data sourced from Opitz et al. (2020) for sample B, and QEMSCAN mineralogy data for samples B and C

Sample	Iron hosting by various minerals						
	Pyrite	Pyrrhotite	Magnetite	Mica	Amphibole	Chlorite	Pyroxene
B	18.6%	3.84%	58.8%	10.9%	3.5%	0.9%	2.4%
C	4.3%	83.5%	1.2%	6.9%	0.9%	2.5%	0.4%



Table A-6 Minerals and corresponding chemical formulae

Mineral	Average formula
Pyrite; Marcasite	FeS ₂
Pyrrhotite	Fe _(1-x) S (0<x<0.17)
Galena	PbS
Sphalerite	ZnS
Chalcopyrite	CuFeS ₂
Arsenopyrite	FeAsS
Calcite	CaCO ₃
Dolomite	CaMg(CO ₃) ₂
Ankerite	Ca(Fe ²⁺ ,Mg,Mn)(CO ₃) ₂
Magnesite	MgCO ₃
Siderite	Fe ²⁺ CO ₃
Rhodochrosite	MnCO ₃
Brucite	Mg(OH) ₂
Melanterite	Fe ²⁺ SO ₄ ·7H ₂ O
Romerite	Fe ²⁺ Fe ³⁺ ₂ (SO ₄) ₄ ·14H ₂ O
Copiapite	Fe ²⁺ Fe ³⁺ ₄ (SO ₄) ₆ (OH) ₂ ·20H ₂ O
Rozenite	Fe ²⁺ (SO ₄)·4H ₂ O
Szomolnokite	FeSO ₄ ·H ₂ O
Jarosite	KFe ₃ (SO ₄) ₂ (OH) ₆
Alunite	KAl ₃ (SO ₄) ₂ (OH) ₆
Goethite	FeO(OH)
Anorthite	CaAl ₂ Si ₂ O ₈
Bytownite	(Ca,Na)(Si,Al) ₄ O ₈
Forsterite	Mg ₂ SiO ₄
Fayalite	Fe ²⁺ ₂ SiO ₄
Diopside	CaMgSi ₂ O ₆
Hedenbergite	CaFe ²⁺ Si ₂ O ₆
Jadeite	Na(Al,Fe ³⁺)Si ₂ O ₆
Spodumene	LiAlSi ₂ O ₆
Bronzite/hypersthene	(Mg,Fe ₂₊) ₂ Si ₂ O ₆
Wollastonite	CaSiO ₃
Nepheline	(Na,K)AlSi ₃ O ₈
Leucite	KAlSi ₂ O ₆
Epidote	Ca ₂ Al ₂ (Fe ³⁺ ,Al)(SiO ₄)(Si ₂ O ₇)O(OH)
Zoisite	Ca ₂ Al ₃ (SiO ₄)(Si ₂ O ₇)O(OH)
Biotite	K(Mg,Fe ²⁺) ₃ AlSi ₃ O ₁₀ (OH,F) ₂
Enstatite	MgSiO ₃
Ferrosilite	(Fe ²⁺ ,Mg)SiO ₃
Augite	(Ca,Na)(Mg,Fe,Al,Ti)(Si,Al) ₂ O ₆
Goethite	Fe ³⁺ O(OH)
Hornblende	Ca ₂ (Mg, Fe, Al) ₅ (Al, Si) ₈ O ₂₂ (OH) ₂
Tremolite	Ca ₂ Mg ₅ Si ₈ O ₂₂ (OH) ₂
Actinolite	Ca ₂ (Mg,Fe ²⁺) ₅ Si ₈ O ₂₂ (OH) ₂
Glaucophane	Na ₂ (Mg ₃ Al ₂)Si ₈ O ₂₂ (OH) ₂
Anthophyllite	Mg ₇ Si ₈ O ₂₂ (OH) ₂
Chrysotile	Mg ₃ Si ₂ O ₅ (OH) ₄
Talc	Mg ₃ Si ₄ O ₁₀ (OH) ₂
Chlorite	(Mg,Fe) ₃ (Si,Al) ₄ O ₁₀ (OH) ₂ ·(Mg,Fe) ₃ (OH) ₆
Orthopyroxene/hypersthene	(Mg,Fe ₂₊) ₂ Si ₂ O ₆

Grunerite	$\text{Fe}^{2+}_7\text{Si}_8\text{O}_{22}(\text{OH})_2$
Annite	$\text{KFe}^{2+}_3\text{AlSi}_3\text{O}_{10}(\text{OH},\text{F})_2$
Albite	$\text{NaAlSi}_3\text{O}_8$
Orthoclase/K-Feldspar	KAlSi_3O_8
Oligoclase	$(\text{Na},\text{Ca})(\text{Si},\text{Al})_4\text{O}_8$
Labradorite	$(\text{Ca},\text{Na})(\text{Si},\text{Al})_4\text{O}_8$
Kaolinite	$\text{Al}_2\text{Si}_2\text{O}_5(\text{OH})_4$
Vermiculite	$(\text{Mg},\text{Fe}^{2+},\text{Al})_3(\text{Al},\text{Si})_4\text{O}_{10}(\text{OH})_{2.4}(\text{H}_2\text{O})$
Montmorillonite	$(\text{Na},\text{Ca})_{0.33}(\text{Al},\text{Mg})_2(\text{Si}_4\text{O}_{10})(\text{OH})_2$
Magnetite	$\text{Fe}^{2+}\text{Fe}^{3+}_2\text{O}_4$
Hematite	Fe_2O_3
Muscovite	$\text{KAl}_2(\text{Si}_3\text{Al})\text{O}_{10}(\text{OH},\text{F})_2$
Quartz	SiO_2
Titanite/Sphene	CaTiSiO_4
Rutile	TiO_2
Zircon	ZrSiO_4